

Quantum Nonequilibrium Physics with Rydberg Atoms

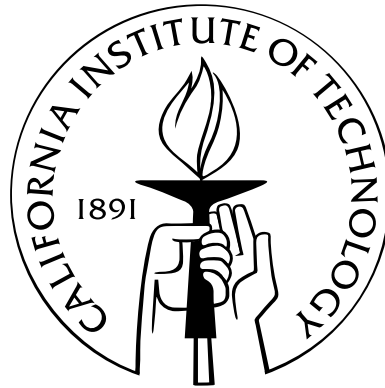
Thesis by

Tony E. Lee

In Partial Fulfillment of the Requirements

for the Degree of

Doctor of Philosophy



California Institute of Technology

Pasadena, California

2012

(Defended May 2, 2012)

© 2012

Tony E. Lee

All Rights Reserved

Acknowledgements

I would like to thank my advisor, Michael Cross, for his mentorship. I learned from him how to ask basic questions when doing research, as well as how to articulate the results in a paper or talk. I appreciate that I could always drop by to ask questions about any kind of physics. I also appreciate the freedom I had to work on some admittedly random problems. Next, I would like to thank Gil Refael for teaching me a lot of new physics and broadening my horizons. In addition, I want to thank Hartmut Häffner, to whom I owe my knowledge of quantum optics. Thanks also to Harvey Newman for his support during college.

I would also like to acknowledge the people that I have had the pleasure of discussing physics with: Oleg Kogan, Milo Lin, Heywood Tam, Olexei Motrunich, Debanjan Chowdhury, Hsin-Hua Lai, Kun Woo Kim, Liyan Qiao, Shankar Iyer, Chang-Yu Hou, Ron Lifshitz, Alexey Gorshkov, Jens Honer, Mark Rudner, Rob Clark, Nikos Daniilidis, and Sankar Narayanan. Thanks to Loly Ekmekjian for her help. Thanks also to Kevin Park, whom I hold responsible for introducing me to Caltech.

I am grateful to my parents and brother for encouraging and supporting my education. Finally, I want to thank Patty for her support over the past few years. Without her, graduate school would have been much less enjoyable.

Abstract

A Rydberg atom is an atom excited to a high energy level, and there is a strong dipole-dipole interaction between nearby Rydberg atoms. While there has been much interest in closed systems of Rydberg atoms, less is known about open systems of Rydberg atoms with spontaneous emission. This thesis explores the latter.

We consider a lattice of atoms, laser-excited from the ground state to a Rydberg state and spontaneously decaying back to the ground state. Using mean-field theory, we study the how the steady-state Rydberg population varies across the lattice. There are three phases: uniform, antiferromagnetic, and oscillatory.

Then we consider the dynamics of the quantum model when mean-field theory predicts bistability. Over time, the system occasionally jumps between a state of low Rydberg population and a state of high Rydberg population. We explain how entanglement and quantum measurement enable the jumps, which are otherwise classically forbidden.

Finally, we let each atom be laser-excited to a short-lived excited state in addition to a Rydberg state. This three-level configuration leads to rich spatiotemporal dynamics that are visible in the fluorescence from the short-lived excited state. The atoms develop strong spatial correlations that change on a long time scale.

Contents

Acknowledgements	iii
Abstract	iv
List of Figures	ix
List of Tables	xi
1 Introduction	1
1.1 Nonequilibrium physics	1
1.2 Examples of nonequilibrium systems	3
1.3 Quantum nonequilibrium systems	4
1.4 Cold atoms	5
1.5 Overview of the thesis	6
2 Quantum trajectory method	8
2.1 Thought experiment	8
2.2 Quantum trajectory method	11
2.3 Two-level atom with laser excitation	13
2.4 Quantum jumps of a three-level atom	15

2.5	Derivation of jump rates for one atom	18
2.6	Interpretation of quantum jumps	22
3	Rydberg atoms	24
3.1	Energy levels	24
3.2	Lifetimes	26
3.2.1	Spontaneous emission	26
3.2.2	Black-body radiation	27
3.3	Interaction in absence of a static electric field	29
3.3.1	Simplified example	30
3.3.2	More-realistic situation	32
3.4	Interaction in presence of a static electric field	34
3.4.1	Single hydrogen atom	34
3.4.2	Interaction of two hydrogen atoms	36
3.4.3	Nonhydrogenic atoms	36
3.5	Rydberg blockade	37
4	Antiferromagnetic phase transition in a nonequilibrium lattice of Rydberg atoms	40
4.1	Model	40
4.2	Mean-field theory	43
4.3	Mean-field results	45
4.4	Original quantum model	49
4.5	Experimental considerations	50

4.6	Conclusion	51
4.A	Mean-field solutions for sublattices	52
4.A.1	Number of uniform fixed points	54
4.A.2	Stability of uniform fixed points	55
4.A.2.1	Stability to symmetric perturbations	56
4.A.2.2	Stability to antisymmetric perturbations	58
4.A.3	Nonuniform fixed points	59
4.A.4	Connection between uniform and nonuniform fixed points . . .	61
4.B	Mean-field solutions for the complete lattice	62
5	Collective quantum jumps of Rydberg atoms	67
5.1	Model	67
5.2	Case of $N = 2$ atoms	70
5.3	Case of $N = 16$ atoms	72
5.4	Experimental considerations	76
5.5	Conclusion	76
6	Spatiotemporal dynamics of quantum jumps with Rydberg atoms	78
6.1	Many-atom model	79
6.2	Case of $\Omega_r \ll \Omega_e^2/\gamma_e$	83
6.3	Case of $\Omega_r = \Omega_e, \Delta_r = 0$	87
6.4	Experimental considerations	88
6.5	Conclusion	89
6.A	Jump rates for two atoms, $\Omega_r \ll \Omega_e^2/\gamma_e$	90

6.B	Jump rates for two atoms, $\Omega_r = \Omega_e, \Delta_r = 0$	94
7	Conclusion	98
	Bibliography	100

List of Figures

1.1	An open system with driving and dissipation	2
1.2	Rayleigh-Bénard convection	4
2.1	Excited-state population over time for a two-level atom that starts in $(g\rangle + e\rangle)/\sqrt{2}$	10
2.2	Level diagram of an atom with laser excitation and spontaneous emission	13
2.3	Quantum trajectory for single atom with laser excitation and spontaneous emission	14
2.4	Level diagram of an atom with three levels	16
2.5	Quantum trajectory of an atom undergoing quantum jumps	17
2.6	Probability that the atom has not emitted a photon by time t , given that it emitted at time 0	19
3.1	Two views of Rydberg blockade	38
4.1	Two sublattices	44
4.2	Bifurcation diagram showing fixed-point solutions as function of Δ	47
4.3	Oscillatory steady-state solution and phase diagram	48
4.4	Numerical solution of master equation for a 1D chain of length $N = 10$	50

5.1	Level diagram and quantum trajectory for $N = 2$ atoms	71
5.2	Photon correlation for two atoms	71
5.3	Mean-field bistability and photon correlation for $N = 16$ atoms	73
5.4	Quantum trajectory of $N = 16$ atoms showing collective quantum jumps	74
5.5	Statistics comparing $N = 4, 8, 16$	76
6.1	Level diagrams for one and two atoms	80
6.2	Quantum trajectory simulations of a chain of $N = 8$ atoms	82
6.3	Quantum trajectory simulations of $N = 2$ atoms	83
6.4	Ratio of $\Gamma^{BD \rightarrow DD}$ to $\Gamma^{BD \rightarrow BB}$	84
6.5	Dynamics of dark regions	86
6.6	Comparison of analytical and numerical values of the jump rates	88

List of Tables

3.1	Properties of Rydberg states	26
-----	--	----

Chapter 1

Introduction

1.1 Nonequilibrium physics

This thesis is about nonequilibrium many-body systems. To clarify what a nonequilibrium system is, it is useful to review what an equilibrium system is. An equilibrium system has certain conserved quantities, such as energy or particle number, which are constant in time [43]. The system explores all the states that are allowed by the values of the conserved quantities. One writes down a thermodynamic potential, from which one calculates properties of the system, like specific heat or susceptibility. There are many powerful tools in statistical mechanics to deal with equilibrium systems.

For example, one type of equilibrium system is the canonical ensemble, which has conserved temperature and particle number. Suppose the system has many possible states that it can be in, each labelled by i and with energy E_i . The system ergodically explores all the possible states in time, but the probability that it is in state i at a given moment is proportional to the Boltzmann factor, $\exp(-k_b E_i/T)$. One writes down a partition function, $Z = \sum_i \exp(-k_b E_i/T)$, and then calculates the free energy, $F = -k_b \log Z$, which is the thermodynamic potential for the canonical ensemble. By

minimizing the free energy, one determines the phase of the system.

In contrast, a nonequilibrium system does not have conserved quantities and hence has no partition function or free energy. This is because it is coupled to its environment through driving and dissipation (Fig. 1.1) [16]. An open system like this is often called a *driven-dissipative* system.¹ The driving and dissipation are such that there are no conserved quantities like energy or temperature. Thus, one cannot use the tools of statistical mechanics that were developed to deal with equilibrium systems. Instead, one needs to look at the underlying dynamical equations of motion.

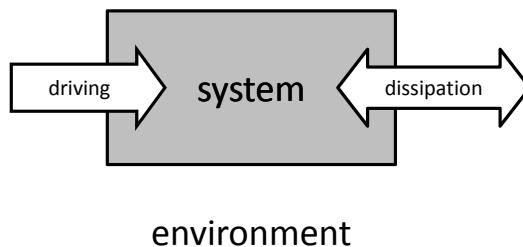


Figure 1.1: An open system with driving and dissipation

People have been interested in nonequilibrium systems for a long time, because there are many phenomena that occur in nonequilibrium that are not possible in equilibrium. The phenomena arise due to the balance of driving and dissipation.

Below, we give some examples.

¹“Nonequilibrium” can also mean something different: the system is not in equilibrium at first, but approaches it as time progresses. An example is a structural glass: the system is stuck in a local minimum of the free energy and takes a very long time to relax to the global minimum [9]. Another example is a system that starts in equilibrium but then undergoes a quench, i.e., a parameter is suddenly changed [67]. After the quench, the system is not in the minimum of the free energy anymore but gradually approaches it. In contrast, a driven-dissipative system never reaches equilibrium.

1.2 Examples of nonequilibrium systems

A good example is the weather. In the absence of any driving, the dissipative processes of heat diffusion and air diffusion would eventually equilibrate the Earth, so that it would have a uniform temperature and hence be described by equilibrium statistical mechanics.

However, the atmosphere is driven by sunlight and the rotation of the Earth. The combination of driving and dissipation leads to gradients of temperature, e.g., the temperature in Los Angeles is different from that in San Diego. There are always temperature gradients, so air is constantly moving around and the atmosphere is permanently nonequilibrium. The fact that it is nonequilibrium leads to fascinating phenomena, like clouds, snow, and thunderstorms, which are not possible in equilibrium.

Another example is Rayleigh-Bénard convection [17]. Suppose there is a thin layer of fluid, and the temperature of the lower surface is set to be permanently higher than the upper surface by an amount ΔT (Fig. 1.2). There are two competing processes: buoyancy causes warmer fluid to rise and cooler fluid to fall, while viscosity inhibits fluid movement. When ΔT is below a threshold, there is no flow. But when ΔT is above the threshold, buoyancy is strong enough to cause the fluid to flow. The interesting thing is that the flow exhibits a spatial pattern: in one region, the flow is clockwise, while in a neighboring region, the flow is counter-clockwise. The fluid spontaneously divides into alternating regions of clockwise and counter-clockwise flow. For even larger ΔT , complicated behaviors such as spatiotemporal chaos appear.

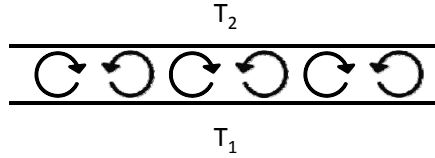


Figure 1.2: Rayleigh-Bénard convection

Rayleigh-Bénard convection is nonequilibrium due to the permanent temperature gradient. Buoyancy acts as driving, since it causes the fluid to move. Dissipation comes from viscosity and heat diffusion. Mathematically, the dynamics of the system are described by the Navier-Stokes equations, which are nonlinear differential equations. The state of the system is determined by the steady state of these equations, as opposed to the minimum of a free energy, as in the canonical ensemble.

1.3 Quantum nonequilibrium systems

The above examples were classical systems. This thesis is about *quantum* nonequilibrium systems. An important difference between quantum and classical systems is quantum measurement, i.e., whenever one measures a quantum system, the wavefunction changes. Quantum measurement is especially important in a nonequilibrium setting: since the system is coupled to the environment, the environment constantly measures the system, causing the wavefunction to decohere.

There has been much work on quantum nonequilibrium physics of single objects, and Chapter 2 reviews some examples for a single atom. In contrast, the bulk of this thesis is about systems of many atoms. A notable feature of quantum many-body systems is entanglement, which is not possible in classical systems.

The general question I am interested in is: *What interesting nonequilibrium phenomena occur in quantum many-body systems, when quantum measurement and entanglement play important roles?* Note that there is no guarantee that anything interesting will happen. If there is too much decoherence, the system will simply end up in a decohered state. However, sometimes the balance of coherence and decoherence leads to interesting effects.

This motivation is different from quantum computing and quantum phase transitions. A quantum computer should be very isolated from the environment, since decoherence destroys quantum information. A quantum phase transition happens in a closed quantum system at zero temperature; the system is in equilibrium and in the ground state. In contrast, this thesis is about what happens when the environmental effects play a central role.

1.4 Cold atoms

A convenient setting to study quantum nonequilibrium physics is cold atoms. Experimentally, one can form a regular lattice of atoms by trapping them in an optical lattice [11]. The lattice can have up to three dimensions and be in various shapes. The atoms are laser-cooled so that they are fixed in position. To make the system nonequilibrium, one shines lasers at the atoms to excite them, and the atoms eventually spontaneously emit photons. Here, driving comes from laser excitation, and dissipation comes from spontaneous emission. Spontaneous emission is convenient because one can detect the photons on a camera or photomultiplier tube and thus

see what is happening in the system. There are many ways to get the atoms to interact and hence become entangled. The bulk of this thesis is based on the Rydberg interaction, which will be introduced in Chapter 3.

Recently, others have also been interested in using cold atoms to study quantum nonequilibrium physics using different approaches. One idea is to immerse an optical lattice of atoms into a Bose-Einstein condensate [20, 21, 83]. The atoms hop between sites of the lattice, and the condensate acts as a phonon bath, leading to dissipation. Another idea is to form an array of optical cavities, each with an atom inside [27, 12, 32, 84]. The cavities are laser-driven, and photons can hop between neighboring cavities. Dissipation is due to the leakage of photons out of the cavities.

1.5 Overview of the thesis

This thesis discusses nonequilibrium physics of Rydberg atoms. Chapter 2 provides background on quantum measurement in the context of spontaneous emission, and Chapter 3 provides background on Rydberg atoms and the interaction between them. Then Chapters 4, 5, and 6 describe three works, which are the main results of the thesis. Chapter 4 describes a nonequilibrium phase transition of Rydberg atoms using mean-field theory [47]. Chapter 5 compares mean-field theory with the actual quantum dynamics, leading to collective quantum jumps [48]. Chapter 6 shows how the Rydberg interaction leads to spatiotemporal dynamics of atomic fluorescence [45].

In the first part of graduate school, I worked on classical nonequilibrium systems. Since those projects are quite different, I have not included them in this thesis. But,

for the record, I worked on synchronization of nonlinear oscillators in one and two dimensions [49, 50], and pattern formation with trapped ions [46].

Chapter 2

Quantum trajectory method

This chapter provides background on quantum measurement in the context of spontaneous emission. It introduces the quantum trajectory method and applies it to a few examples.

2.1 Thought experiment

Suppose there is an atom with two levels: ground state $|g\rangle$ and excited state $|e\rangle$. The atom is coupled to the environment, and that coupling manifests itself as spontaneous emission: with rate γ , the excited state decays to the ground state and emits a photon at the same time. Suppose the environment also detects the emitted photon with 100% efficiency. (Any experiment will inevitably be surrounded by walls which absorb the photon. Or one can imagine surrounding the atom with photomultiplier tubes.)

Let the wave function of the atom start in a superposition:

$$|\psi(t)\rangle = \alpha|g\rangle + \beta|e\rangle. \tag{2.1}$$

The question is: after a short time interval dt , what is the wave function, $|\psi(t + dt)\rangle$? In that time interval, two things can happen: either a photon is detected or not. If a photon is detected, the wave function is projected into the ground state: $|\psi(t + dt)\rangle = |g\rangle$. But if a photon is not detected, it is not obvious what to do. One might think that since nothing happened, the wave function is still in the original state, Eq. (2.1). But that turns out to be incorrect, because even the non-detection of a photon is a measurement, and the wave function must be updated accordingly.

Let us examine this problem more carefully. In addition to the atomic wave function, we keep track of an electromagnetic mode near the atom. In reality, there is an infinite number of modes around the atom, but for simplicity we lump them all into one mode. The state of this mode is $|n\rangle$, where n is the number of photons in it. Suppose there are no photons at the beginning:

$$|\psi(t)\rangle = (\alpha|g\rangle + \beta|e\rangle)|0\rangle. \quad (2.2)$$

In the time interval dt , the probability that the atom decays is $p = \gamma|\beta|^2 dt$. Note that $p \ll 1$. The wave function then evolves to

$$|\psi(t + dt)\rangle = \alpha|g\rangle|0\rangle + \beta \left(1 - \frac{\gamma dt}{2}\right) |e\rangle|0\rangle + \sqrt{p}|g\rangle|1\rangle. \quad (2.3)$$

In other words, with probability p , the excited state decays to the ground state, emitting a photon in the process. Equation (2.3) makes intuitive sense, but it can be derived rigorously with the Weisskopf-Wigner approximation [76]. (To derive this

rigorously, one needs to keep track of all the electromagnetic modes instead of just one.)

At this point, the environment detects whether or not there is a photon. If it detects a photon, the $|1\rangle$ component of Eq. (2.3) is projected out:

$$|\psi(t + dt)\rangle = |g\rangle|1\rangle. \quad (2.4)$$

If no photon is detected, the $|0\rangle$ component is projected out (and normalized):

$$|\psi(t + dt)\rangle = \alpha \left(1 + \frac{\gamma|\beta|^2 dt}{2}\right) |g\rangle|0\rangle + \beta \left(1 - \frac{\gamma|\alpha|^2 dt}{2}\right) |e\rangle|0\rangle. \quad (2.5)$$

Comparing Eqs. (2.2) and (2.5), we see that the excited-state population decreased a little, while the ground-state population increased a little. In other words, *the non-detection of a photon shifts the atom towards the ground state in a nonunitary way.*

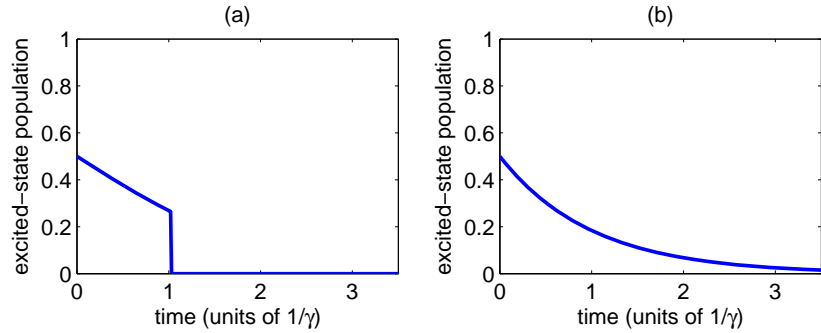


Figure 2.1: Excited-state population over time for a two-level atom that starts in $(|g\rangle + |e\rangle)/\sqrt{2}$. (a) Single experiment. (b) Average over many experiments

Figure 2.1(a) shows an example of a single experiment. It plots the population of the excited state over time. The wave function starts out in $(|g\rangle + |e\rangle)/\sqrt{2}$. For a

while, no photon is detected, so the excitation decreases. At time $t \approx 1/\gamma$, a photon is detected, so the atom collapses to the ground state and stays there. Thus, in a single experiment, the wave function can change discontinuously. But averaging over many experiments results in a smooth curve (Fig. 2.1(b)), since the atom emits at a different time in each experiment.

Suppose again that the wave function starts in a superposition, $\alpha|g\rangle + \beta|e\rangle$. There is a probability $|\alpha|^2$ that the atom never emits a photon, since that is the ground-state population at the beginning. During an experiment, in which the atom never emits, the excited-state population decays smoothly to zero over time. In other words, if no photon is ever detected, the accumulation of many null measurements projects the atom into $|g\rangle$ [61].

2.2 Quantum trajectory method

The above considerations led people to come up with the quantum trajectory method [18, 61]. (Sometimes it is called the Monte Carlo wave function method or quantum-jump approach.) It is an algorithm to evolve the wave function in the presence of a Hamiltonian H as well as spontaneous emission. H includes coherent processes, such as laser excitation or interaction between atoms. Below, we explain the method in the context of a two-level atom, but it is straightforward to generalize it to an arbitrary system.¹

¹The trajectory dynamics depend on how the environment measures the emitted light. Since atomic fluorescence is usually measured with a photomultiplier tube or camera, we assume in this thesis that the environment counts individual photons. Another measurement technique is homodyne detection, which measures the quadrature of light and is often used in cavity QED. The quantum

One starts with the atomic wave function at time t , $|\psi(t)\rangle = \alpha|g\rangle + \beta|e\rangle$ and calculates the probability of an emission in time interval dt , $p = \gamma|\beta|^2 dt$. With probability p , one decides that the atom emits, in which case $|\psi(t+dt)\rangle = |g\rangle$. With probability $1-p$, the atom does not emit, in which case one evolves $|\psi(t)\rangle$ using an effective Hamiltonian: $|\psi(t+dt)\rangle = (1 - iH_{\text{eff}} dt)|\psi(t)\rangle$, where $H_{\text{eff}} = H - \frac{i\gamma}{2}|e\rangle\langle e|$. The non-Hermitian part of H_{eff} is a shortcut to account for the fact that the non-detection of a photon decreases the excited-state population. At this point, one normalizes $|\psi(t+dt)\rangle$ to 1 and repeats the process for the next time step, and this cycle repeats over and over.

The quantum trajectory method simulates what happens in a single experiment. It is a Monte Carlo approach, since each trajectory is different. The method can be shown to be equivalent to the Lindblad master equation for the density matrix ρ [18, 61]:

$$\frac{d}{dt}\rho = -i[H, \rho] + \frac{\gamma}{2}(-|e\rangle\langle e|\rho - \rho|e\rangle\langle e| + 2|g\rangle\langle e|\rho|g\rangle\langle e|). \quad (2.6)$$

The difference is that the quantum trajectory method describes how a single wave function evolves in a single experiment, while the master equation describes how an ensemble of wave functions evolves. Although they are equivalent, quantum trajectories sometimes provide a lot of insight into what is happening in the system, which might not be obvious from the master equation. In particular, quantum trajectories provide examples of photon signals that an experimentalist would measure. This trajectory method for homodyne detection is quite different from that of photon counting, even though they are described by the same master equation [65].

thesis will show many quantum trajectories.

The quantum trajectory method can even be used to solve the master equation, since the two are equivalent. Sometimes, it is computationally faster to average over many quantum trajectories than to directly integrate the master equation [18, 61].

2.3 Two-level atom with laser excitation

Here, we apply the quantum trajectory method to a two-level atom in the presence of laser excitation and spontaneous emission. This is the simplest quantum nonequilibrium system. Driving comes from the laser, while dissipation comes from spontaneous emission. This textbook problem is usually solved using the master equation [60], but it is interesting to view it from a quantum-trajectory point of view.

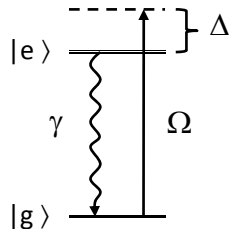


Figure 2.2: Level diagram of an atom with laser excitation and spontaneous emission

The Hamiltonian is²

$$H = -\Delta|e\rangle\langle e| + \frac{\Omega}{2}(|g\rangle\langle e| + |e\rangle\langle g|), \quad (2.7)$$

²Throughout this thesis, we use the interaction picture, rotating-wave approximation, and let $\hbar = 1$.

where Δ is the laser detuning and Ω is the Rabi frequency, which depends on the laser intensity (Fig. 2.2). The linewidth γ accounts for spontaneous emission. An example trajectory is shown in Fig. 2.3, which plots the excited-state population vs. time. The atom starts in the ground state and emits photons at various times. Interestingly, after a long period without a photon emission, the wave function approaches a steady state and the excitation levels off. Physically, this is due to the balance of two processes: laser driving increases the excitation, while the non-detection of photons decreases the excitation.

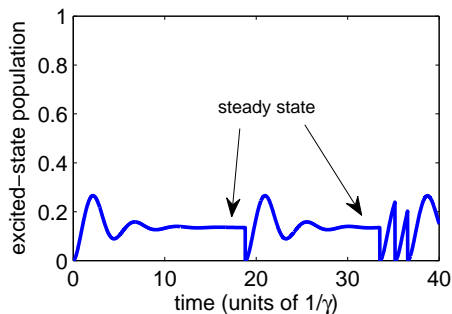


Figure 2.3: Quantum trajectory for single atom with laser excitation and spontaneous emission. The parameters are $\Omega = \Delta = \gamma$. Photons are emitted at $t/\gamma = 18.8, 33.5, 35.2,$ and 36.6 .

Mathematically, the steady state is because of the following. In the absence of a photon emission, the wave function evolves with $H_{\text{eff}} = H - \frac{i\gamma}{2}|e\rangle\langle e|$:

$$i\frac{d}{dt}|\psi(t)\rangle = H_{\text{eff}}|\psi(t)\rangle. \quad (2.8)$$

The general solution to this differential equation is given by the eigenvalues λ_i and

eigenvectors $|u_i\rangle$ of H_{eff} :

$$|\psi(t)\rangle = c_1 e^{-i\lambda_1 t} |u_1\rangle + c_2 e^{-i\lambda_2 t} |u_2\rangle, \quad (2.9)$$

where c_1 and c_2 are determined by the initial condition, $|\psi(0)\rangle = |g\rangle$. Since H_{eff} is non-Hermitian, λ_1 and λ_2 are complex, so both terms in Eq. (2.9) decay. In general, one of the eigenvalues has a less negative imaginary part, so that term decays more slowly than the other. Thus, after a long time without a photon detection, only that term remains, and it corresponds to the steady-state wave function seen in Fig. 2.3. This effect will be important in Chapters 5 and 6.

2.4 Quantum jumps of a three-level atom

A good application of quantum trajectories is to quantum jumps of a three-level atom [15, 13, 65]. This section summarizes the main results, while Section 2.5 reviews the derivation of the jump rates, and Section 2.6 provides a physical interpretation of quantum jumps in terms of quantum measurement.

Consider an atom with three levels: ground state $|g\rangle$, short-lived excited state $|e\rangle$, and metastable state $|r\rangle$ (Fig. 2.4). A laser drives the strong transition $|g\rangle \rightarrow |e\rangle$, while another drives the weak transition $|g\rangle \rightarrow |r\rangle$. The strong transition acts as a measurement of whether or not the atom is in $|r\rangle$. When the atom is not in $|r\rangle$, the atom is repeatedly excited to $|e\rangle$ and spontaneously emits photons. Occasionally the atom is excited to $|r\rangle$ and stays there, and the fluorescence from the strong transition

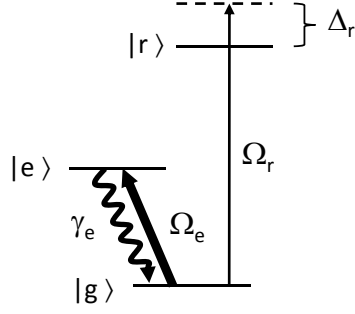


Figure 2.4: Level diagram of an atom with three levels

turns off. Eventually, the atom returns to $|g\rangle$, and the fluorescence turns back on. Thus, the fluorescence signal of the strong transition exhibits bright and dark periods, and the occurrence of a dark period implies that the atom is in $|r\rangle$. The transitions between the bright and dark periods are quite sudden and reflect quantum jumps to and from $|r\rangle$. Quantum jumps are a good example of how a quantum nonequilibrium system can have nontrivial dynamics.

The Hamiltonian for the system is

$$H = \frac{\Omega_e}{2}(|g\rangle\langle e| + |e\rangle\langle g|) + \frac{\Omega_r}{2}(|g\rangle\langle r| + |r\rangle\langle g|) - \Delta_e|e\rangle\langle e| - \Delta_r|r\rangle\langle r|, \quad (2.10)$$

where Δ_e and Ω_e are the laser detuning and Rabi frequency of the strong transition, while Δ_r and Ω_r are the corresponding quantities for the weak transition. In the absence of spontaneous emission, Eq. (2.10) would completely describe the system. However, the excited states have lifetimes given by their linewidths, γ_e and γ_r .

For simplicity, we make the following assumptions on the parameters. We set

$\Delta_e = 0$, so the strong transition is on resonance. We also set $\gamma_r = 0$, so the metastable state has an infinite lifetime. It is straightforward to extend the analysis to nonzero $\Delta_e = 0$ and $\gamma_r = 0$.

Figure 2.5 shows an example quantum trajectory. The population of the Rydberg state jumps between a low value and a high value.

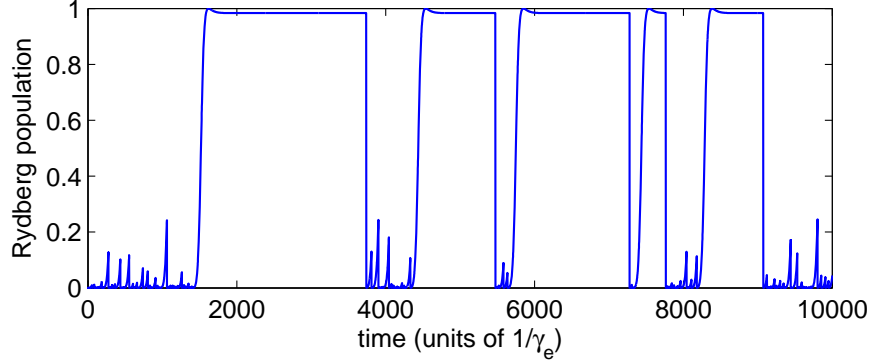


Figure 2.5: Quantum trajectory of an atom undergoing quantum jumps. $\Omega_e = 0.2\gamma_e$, $\Omega_r = 0.005\gamma_e$, $\Delta_e = \Delta_r = \gamma_r = 0$.

Well-defined jumps appear in the fluorescence signal when a bright period consists of many emitted photons while a dark period consists of the absence of many photons. For a single atom, this happens when $\Omega_r \ll \Omega_e^2/\gamma_e$ in the case of $\Delta_r = 0$ [13]. The transition rate from a dark period to a bright period is [65]

$$\Gamma^{D \rightarrow B}(\Delta_r) = \frac{\gamma_e \Omega_e^2 \Omega_r^2}{16\Delta_r^4 + 4\Delta_r^2(\gamma_e^2 - 2\Omega_e^2) + \Omega_e^4}, \quad (2.11)$$

and the rate from a bright period to a dark period is

$$\Gamma^{B \rightarrow D}(\Delta_r) = \frac{\gamma_e^2 + 4\Delta_r^2}{\gamma_e^2 + 2\Omega_e^2} \Gamma^{D \rightarrow B}(\Delta_r), \quad (2.12)$$

where B and D denote bright and dark periods. An important feature of these equations is that both rates are maximum when $\Delta_r = 0$ since the strength of the weak transition is maximum there. When $\Delta_r = 0$, both rates are approximately $\gamma_e \Omega_r^2 / \Omega_e^2$. This depends inversely on Ω_e , because increasing Ω_e is equivalent to measuring the atomic state more frequently; this inhibits transitions to and from $|r\rangle$, similar to the quantum Zeno effect [36].

Quantum jumps have been observed in many settings, such as trapped ions [62, 74, 8], photons [28], electrons [85], and superconducting qubits [87]. In these experiments, the object being observed is a single particle or can be described by a single degree of freedom. In Chapters 5 and 6, we discuss quantum jumps involving many Rydberg atoms.

2.5 Derivation of jump rates for one atom

This section reviews the derivation of jump rates for one atom. We essentially reproduce the derivation in Refs. [13, 68, 65], because we need to refer back to it in Chapter 6, and it is convenient to see it in our notation. We use the quantum-trajectory approach, which is based on the wave function, to account for spontaneous emission, but it is also possible to base the calculation on the density matrix [42].

When an atom exhibits quantum jumps, the fluorescence signal has bright periods, in which the photons are closely spaced in time, and dark periods, in which no photons are emitted for a while. The goal is to calculate the transition rate from a bright period to a dark period and vice versa. The important quantity is the time interval between

successive emissions [13]. During a bright period, the intervals are short, but a dark period is an exceptionally long interval. Suppose one has the function $P_0(t)$, which is the probability that the atom has not emitted a photon by time t , given that it emitted at time 0. $P_0(t)$ decreases monotonically as t increases (Fig. 2.6). When the parameters are such that there are well-defined quantum jumps, $P_0(t)$ decreases rapidly to a small value for small t , but has a long tail for large t . This reflects the fact that the time between emissions is usually short (bright period), but once in a while it is very long (dark period). Note that each emission is an independent event, due to the fact that the wave function always returns to $|g\rangle$ after an emission.

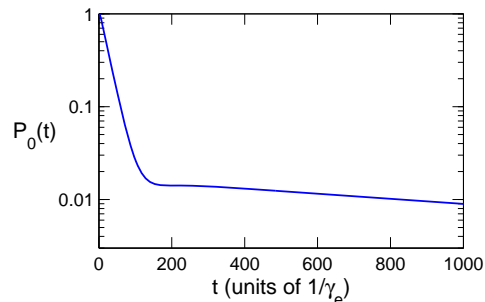


Figure 2.6: Probability that the atom has not emitted a photon by time t , given that it emitted at time 0. Same parameters as Fig. 2.5: $\Omega_e = 0.2\gamma_e$, $\Omega_r = 0.005\gamma_e$, $\Delta_e = \Delta_r = \gamma_r = 0$.

We write $P_0(t) = P_{\text{short}}(t) + P_{\text{long}}(t)$ to separate the short and long time-scale parts. The long tail is given by $P_{\text{long}}(t) = p \exp(-\Gamma^{D \rightarrow B} t)$, where p is the probability that a given interval is long enough to be a dark period, and $\Gamma^{D \rightarrow B}$ is the transition rate from a dark period to a bright period. In other words, $1/\Gamma^{D \rightarrow B}$ is the average duration of a dark period.

To calculate $P_0(t)$, we follow the evolution of the wave function $|\psi(t)\rangle$, given that the atom has not emitted a photon yet. This is found by evolving $|\psi(t)\rangle$ with a non-

Hermitian Hamiltonian $H_{\text{eff}} = H - i\frac{\gamma_e}{2}|e\rangle\langle e|$. The non-Hermitian term accounts for the population that emits a photon, hence dropping out of consideration [13]. Thus, $P_0(t) = \langle\psi(t)|\psi(t)\rangle$.

In the basis $\{|g\rangle, |e\rangle, |r\rangle\}$, the matrix form of H_{eff} is

$$H_{\text{eff}} = \begin{pmatrix} 0 & \frac{\Omega_e}{2} & \frac{\Omega_r}{2} \\ \frac{\Omega_e}{2} & -i\frac{\gamma_e}{2} & 0 \\ \frac{\Omega_r}{2} & 0 & -\Delta_r \end{pmatrix}. \quad (2.13)$$

As stated in Section 2.4, we assume $\Delta_e = \gamma_r = 0$. We want to solve the differential equation $i\frac{d}{dt}|\psi(t)\rangle = H_{\text{eff}}|\psi(t)\rangle$ given the initial condition $|\psi(0)\rangle = |g\rangle$. The general solution is $|\psi(t)\rangle = \sum_n c_n e^{-i\lambda_n t} |u_n\rangle$, where λ_n and $|u_n\rangle$ are the eigenvalues and eigenvectors of H_{eff} , and c_n is determined from the initial condition $|g\rangle = \sum_n c_n |u_n\rangle$.

We calculate the eigenvalues and eigenvectors perturbatively in Ω_r , which is assumed to be small. (Note that since H_{eff} is non-Hermitian, perturbation theory is different from the usual Hermitian case [81].) All three eigenvalues have negative imaginary parts, which leads to the nonunitary decay. It turns out that the imaginary part of one of the eigenvalues, which we call λ_3 , is much less negative than the other two. This means that the $|u_1\rangle$ and $|u_2\rangle$ components in $|\psi(t)\rangle$ decay much faster than the $|u_3\rangle$ component. After a long time without a photon emission, $|\psi(t)\rangle$ contains only $|u_3\rangle$. Thus, λ_3 corresponds to the long tail of $P_0(t)$.

To second order in Ω_r [13, 68],

$$\lambda_3 = -\Delta_r + \frac{\Omega_r^2(-2\Delta_r + i\gamma_e)}{8\Delta_r^2 - 2\Omega_e^2 - 4i\gamma_e\Delta_r}. \quad (2.14)$$

To first order in Ω_r ,

$$|u_3\rangle = \frac{\Omega_r(-2\Delta_r + i\gamma_e)}{4\Delta_r^2 - \Omega_e^2 - 2i\gamma_e\Delta_r}|g\rangle + \frac{\Omega_e\Omega_r}{4\Delta_r^2 - \Omega_e^2 - 2i\gamma_e\Delta_r}|e\rangle + |r\rangle \quad (2.15)$$

$$c_3 = \frac{\Omega_r(-2\Delta_r + i\gamma_e)}{4\Delta_r^2 - \Omega_e^2 - 2i\gamma_e\Delta_r}. \quad (2.16)$$

Since $|u_3\rangle$ consists mainly of $|r\rangle$, the occurrence of a dark period implies, as expected, that the atom is in $|r\rangle$. (However, note that the atom is not completely in $|r\rangle$. In fact, the dark period ends when the small $|e\rangle$ component in $|u_3\rangle$ decays and emits a photon [65].)

We can now construct $P_{\text{long}}(t)$:

$$p = |c_3|^2 = \frac{\Omega_r^2(\gamma_e^2 + 4\Delta_r^2)}{16\Delta_r^4 + 4\Delta_r^2(\gamma_e^2 - 2\Omega_e^2) + \Omega_e^4} \quad (2.17)$$

$$\Gamma^{D \rightarrow B} = -2 \text{Im } \lambda_3 = \frac{\gamma_e\Omega_e^2\Omega_r^2}{16\Delta_r^4 + 4\Delta_r^2(\gamma_e^2 - 2\Omega_e^2) + \Omega_e^4}. \quad (2.18)$$

Then, instead of finding $P_{\text{short}}(t)$ explicitly, we use a shortcut [65]. During a bright period, there is negligible population in $|r\rangle$, so the atom is basically a two-level atom driven by a laser with Rabi frequency Ω_e . Thus, to lowest order in Ω_r , the emission

rate Γ_{short} during a bright period is the same as a two-level atom [60]:

$$\Gamma_{\text{short}} = \frac{\gamma_e \Omega_e^2}{\gamma_e^2 + 2\Omega_e^2}. \quad (2.19)$$

However, each emission in a bright period has a small probability p of taking a long time, in which case the bright period ends. Thus, the transition rate from a bright period to a dark period is

$$\Gamma^{B \rightarrow D} = p \Gamma_{\text{short}} = \frac{\gamma_e^2 + 4\Delta_r^2}{\gamma_e^2 + 2\Omega_e^2} \Gamma^{D \rightarrow B}. \quad (2.20)$$

The jumps are well-defined when a bright or dark period is much longer than the typical emission time during a bright period: $\Gamma^{B \rightarrow D}, \Gamma^{D \rightarrow B} \ll \Gamma_{\text{short}}$. When $\Delta_r = 0$ and $\Omega_e \ll \gamma_e$, this condition becomes $\Omega_r \ll \Omega_e^2/\gamma_e$ [13].

2.6 Interpretation of quantum jumps

The previous section contained a lot of math, so it is worthwhile to clarify the physics of what is happening. Suppose the atom starts out bright, so it cycles back and forth between $|g\rangle$ and $|e\rangle$. The transition to a dark period occurs when the atom happens to not emit a photon for a while. The non-detection of photons projects the atom into $|r\rangle$. In other words, the accumulation of many null measurements means that the atom must be in the state that does not emit, which is $|r\rangle$. To be precise, the atom is projected into $|u_3\rangle$ (Eq. (2.15)), which is the slowest-decaying eigenstate of H_{eff} . This is similar to the steady-state wave function discussed in Section 2.3.

However, $|u_3\rangle$ does not consist completely of $|r\rangle$, because there are small components of $|g\rangle$ and $|e\rangle$. The dark period ends when the $|e\rangle$ component in $|u_3\rangle$ happens to finally emit, projecting the atom into $|g\rangle$. At this point, the atom is repeatedly excited to $|e\rangle$, emits photons, and is bright again.

Note that during the transition to a dark period, the wave function evolves continuously towards the metastable state [65]. In contrast, during the transition to a bright period, the wave function suddenly collapses to $|g\rangle$.

Chapter 3

Rydberg atoms

A Rydberg atom is an atom with an electron excited to a high principal quantum number n . The high n leads to exaggerated atomic properties, including a strong interaction between two nearby Rydberg atoms. This chapter describes Rydberg atoms and the interaction between them.

3.1 Energy levels

Rydberg atoms are usually studied in the context of alkali atoms, which have a single valence electron and hence relatively simple level diagrams. Consider, for example, rubidium, which has a single valence electron and a core, which consists of 36 electrons in filled bands and 37 protons. When the valence electron is far from the core, the core appears as a point charge of +1. Thus, if the electron's orbit stays far from the core, the energy levels are the same as in hydrogen.

On the other hand, when the electron is near the core, it sees how the charge is distributed in space. For example, when the electron is inside the core, it sees the +37 charge of the nucleus, which increases the binding energy and decreases the

total energy. In addition, the electron polarizes the core, which also decreases the energy. Thus, when the electron's orbit is close to the core, the energy levels differ significantly from those of hydrogen.

The energy of a Rydberg state nl is [26]:

$$E_{nl} = -\frac{\text{Ry}}{(n - \delta_l)^2} \quad (3.1)$$

where Ry is the Rydberg constant. δ_l is a quantum defect that depends on the orbital angular momentum l , and it accounts for deviations due to the finite core size. When $\delta_l = 0$, Eq. (3.1) is the usual formula for hydrogen. The quantum defect is usually determined empirically. For rubidium, $\delta_0 = 3.13$, $\delta_1 = 2.64$, $\delta_2 = 1.35$, and $\delta_3 = 0.016$ [54, 31]. As l increases, the electron spends less time near the core, and hence the atom behaves more like hydrogen. Note that the Rydberg levels are also shifted by fine structure [78], which is not included in Eq. (3.1). Hyperfine splitting is relatively small for Rydberg states, so it is usually ignored [73].

Using quantum defect theory, one can construct the wavefunctions of the Rydberg states [26]. An important application of the wavefunctions is to calculate the dipole matrix elements between different atomic states. Instead of going through the calculation, we summarize the results in Table 3.1.

Property	Expression	n dependence
Binding energy	E_n	n^{-2}
Level spacing	$E_n - E_{n-1}$	n^{-3}
Orbital radius	$\langle nl r nl\rangle$	n^2
Dipole matrix element between low-lying state and Rydberg state	e.g. $\langle 5P r nS\rangle$	$n^{-3/2}$
Dipole matrix element between two Rydberg states	e.g. $\langle nP r nS\rangle$	n^2
Radiative lifetime	τ_{nl}^0	n^3

Table 3.1: Properties of Rydberg states

3.2 Lifetimes

The lifetime τ_{nl} of a Rydberg state is limited by two factors: spontaneous emission and black-body radiation. The two contributions can be written as

$$\frac{1}{\tau_{nl}} = \frac{1}{\tau_{nl}^0} + \frac{1}{\tau_{nl}^{bb}}, \quad (3.2)$$

where τ_{nl}^0 is the lifetime due to spontaneous emission only and τ_{nl}^{bb} is the lifetime due to black-body radiation only. At 0 K, there is no black-body radiation, so $\tau_{nl} = \tau_{nl}^0$.

3.2.1 Spontaneous emission

In a spontaneous emission event, the atom decays to a state of lower energy and emits a photon that carries away the energy difference. The rate of spontaneous decay from nl to $n'l'$ is given by the Einstein A coefficient [26],

$$A_{n'l',nl} = \frac{e^2 \omega_{n'l',nl}^3}{3\pi\epsilon_0 \hbar c^3} \frac{l_{\max}}{2l+1} |\langle n'l'|r|nl\rangle|^2, \quad (3.3)$$

where $\omega_{n'l',nl}$ is the frequency difference of the two states, and l_{\max} is the larger of l and l' . We are only interested in dipole-allowed transitions ($l' = l \pm 1$). The dipole-forbidden transitions have much smaller rates. The lifetime of a nl state is the reciprocal of the sum of decay rates to all possible $n'l'$ states:

$$\tau_{nl}^0 = \frac{1}{\sum_{n'l'} A_{n'l',nl}}. \quad (3.4)$$

Note that each $A_{n'l',nl}$ is proportional to $\omega_{n'l',nl}^3$. It turns out that the decay from nl is dominated by transitions to the lowest possible values of n' , because $\omega_{n'l',nl}$ is maximum for those n' [26]. The $\omega_{n'l',nl}^3$ factor outweighs the fact that the matrix element $\langle n'l'|r|nl\rangle$ is small for low n' . For example, the ground state of rubidium is $5S$, so nS decays mostly to $5P$ and $6P$, while nP decays mostly to $5S$, $6S$, and $4D$ [19].

For the transitions from nl to low-lying $n'l'$, as n increases, $\omega_{n'l',nl}$ approaches a constant due to the form of the energy equation (Eq. (3.1)). Thus, for large n , $A_{n'l',nl}$ depends only on the matrix elements from nl to low-lying $n'l'$. As shown in Table 3.1, the dipole matrix elements scale as $n^{-3/2}$. Thus for large n ,

$$\tau_{nl}^0 \sim n^3. \quad (3.5)$$

3.2.2 Black-body radiation

Rydberg states are much more sensitive to black-body radiation than normal states. This is because the energy spacing between Rydberg states is small, so at room

temperature, there are many black-body photons resonant with transitions between Rydberg states. In addition, the matrix elements between Rydberg states are large. The effect of black-body radiation is to transfer the atom from a Rydberg state to nearby Rydberg states.

Recall that in equilibrium at temperature T , an electromagnetic mode of frequency ω contains $N(\omega)$ photons [43]:

$$N(\omega) = \frac{1}{e^{\hbar\omega/k_bT} - 1}. \quad (3.6)$$

When $\hbar\omega \ll k_bT$, $N(\omega) \approx k_bT/\hbar\omega$. Thus, as T increases, the mode is more populated. The effect of black-body radiation on an atom in state nl is twofold: (i) a black-body photon can induce stimulated emission to a lower state $n'l'$; (ii) the atom can absorb a photon to go to a higher state $n'l'$. Both rates are given by [26]:

$$K_{n'l',nl} = A_{n'l',nl}N(\omega_{n'l',nl}), \quad (3.7)$$

where $A_{n'l',nl}$ is given by Eq. (3.3). The frequency dependence of $K_{n'l',nl}$ differs from that of $A_{n'l',nl}$ due to the additional $N(\omega)$ factor. As a result, black-body radiation tends to cause transitions to nearby Rydberg states ($n' \approx n$), in contrast to spontaneous emission, which causes transitions to low-lying states.

By summing over all possible $n'l'$, one finds the approximate relation [26]

$$\tau_{nl}^{bb} = \frac{3\hbar n^2}{4\alpha^3 k_b T}. \quad (3.8)$$

Note that τ_{nl}^0 scales as n^3 while τ_{nl}^{bb} scales as n^2 . This means that as n increases, the overall lifetime τ increases, but the contribution from black-body radiation increasingly dominates over that of spontaneous emission.

More precise estimates for τ_{nl} are tabulated in Ref. [10]. In general, black-body radiation interferes with experiments people want to do, since it transfers the atom to Rydberg states that are not coupled to laser light. Black-body effects can be minimized by working at cryogenic temperatures, as is done in some experiments [69].

3.3 Interaction in absence of a static electric field

The interaction between Rydberg atoms can be a confusing subject because it can take different forms, depending on the experimental setup. In this section, we discuss the interaction when there is no external static electric field. In Section 3.4, we discuss the interaction in the presence of a static electric field.

Suppose there are two atoms, each with one valence electron, and let the atoms be separated by a distance R . The dipole-dipole interaction between them is [37]

$$V_{dd} = \frac{e^2}{4\pi\epsilon_0 R^3} [\vec{r}_1 \cdot \vec{r}_2 - 3(\vec{r}_1 \cdot \hat{R})(\vec{r}_2 \cdot \hat{R})], \quad (3.9)$$

where \vec{r}_1 and \vec{r}_2 are the positions of the two valence electrons relative to their nuclei, and \hat{R} is a unit vector that points from one to the other. In the absence of an electric field, an atom in a parity eigenstate does not have a permanent dipole moment, so

classically there would be no interaction between the two atoms. However, there is a quantum mechanical interaction, because quantum fluctuations induce momentary dipole moments in the atoms that interact with each other.

In the absence of the dipole-dipole interaction, the eigenstates of the system are product states of the two atoms, denoted by $|n'l', n''l''\rangle$. However, the operator V_{dd} couples each two-atom state to all other two-atom states allowed by the dipole selection rules. Thus, in the presence of the interaction, the eigenstates of the two-atom system are mixtures of the original $|n'l', n''l''\rangle$ states.

3.3.1 Simplified example

We illustrate the interaction with a simple example, while Section 3.3.2 describes the more-realistic situation. Due to spin-orbit coupling, a Rydberg state is specified by four quantum numbers: n, l, j, m_j . But for simplicity, we only keep track of n and l . Consider the state $|nl, nl\rangle$, which has both atoms in the same Rydberg state. We describe the effect of the interaction for the case when $|nl, nl\rangle$ couples to only one state, denoted by $|n'l', n''l''\rangle$. Let $\delta = E_{n'l'} + E_{n''l''} - 2E_{nl}$ be the energy difference between the two two-atom states. In the $\{|nl, nl\rangle, |n'l', n''l''\rangle\}$ basis, the Hamiltonian is

$$H = \begin{pmatrix} 0 & \langle nl, nl | V_{dd} | n'l', n''l'' \rangle \\ \langle n'l', n''l'' | V_{dd} | nl, nl \rangle & \delta \end{pmatrix}. \quad (3.10)$$

The eigenstates of H are mixtures of $|nl, nl\rangle$ and $|n'l', n''l''\rangle$, but in the limit of small $|\langle n'l', n''l''|V_{dd}|nl, nl\rangle|$, one eigenstate corresponds asymptotically to $|nl, nl\rangle$, while the other to $|n'l', n''l''\rangle$. We are interested in the one that corresponds to $|nl, nl\rangle$ since that is the experimentally relevant one (Section 3.5). The energy of that eigenstate is given by its eigenvalue:

$$V = \frac{\delta - \text{sgn}(\delta)\sqrt{\delta^2 + 4|\langle n'l', n''l''|V_{dd}|nl, nl\rangle|^2}}{2}. \quad (3.11)$$

Since $|nl, nl\rangle$ originally had zero energy, V is the level shift that it experiences due to the interaction.

Recall that $V_{dd} \sim R^{-3}$. Consider first the limit $|\langle n'l', n''l''|V_{dd}|nl, nl\rangle| \ll \delta$, which corresponds to large R . The level shift becomes

$$V \approx -\frac{|\langle n'l', n''l''|V_{dd}|nl, nl\rangle|^2}{\delta}. \quad (3.12)$$

For large n , the dipole matrix element between nearby Rydberg levels, such as $\langle nP|r|nS\rangle$, scales as n^2 . Thus, $|\langle n'l', n''l''|V_{dd}|nl, nl\rangle|$ contains two factors of n^2 , one for each atom. Also, δ scales as n^{-3} , since that is how the characteristic level spacing scales. For large n ,

$$|V| \sim \frac{n^{11}}{R^6}. \quad (3.13)$$

Then consider the limit $|\langle n'l', n''l'' | V_{dd} | nl, nl \rangle| \gg \delta$, which corresponds to small R :

$$V \approx -\text{sgn}(\delta) \frac{|\langle n'l', n''l'' | V_{dd} | nl, nl \rangle|}{R^3}, \quad (3.14)$$

which scales for large n as

$$|V| \sim \frac{n^4}{R^3}. \quad (3.15)$$

One can define a crossover distance R_c given by when $|\langle n'l', n''l'' | V_{dd} | nl, nl \rangle| \approx \delta$.

When $R > R_c$, the interaction has the van der Waals form in Eq. (3.13). When

$R < R_c$, the interaction has the dipolar form in Eq. (3.15). The scaling with n shows

that the interaction between Rydberg atoms can be very strong.

3.3.2 More-realistic situation

The above example was simplified to bring out the main points. In reality, due to spin-orbit coupling, one must also specify a state's total angular momentum j and magnetic quantum number m_j . Another simplification we made above was that $|nl, nl\rangle$ couples to only one state. To accurately calculate the level shift, one needs to include the contribution from all possible states¹, which is most conveniently done with second-order perturbation theory. Thus, the level shift that $|nljm_j, nljm_j\rangle$ experiences is

¹But the level shift is often dominated by only a few two-atom states that are close in energy. For instance, $|60p_{3/2}, 60p_{3/2}\rangle$ couples most strongly to $|60s_{1/2}, 61s_{1/2}\rangle$ [73].

actually

$$V \approx - \sum_{\substack{n',l',j',m'_j \\ n'',l'',j'',m''_j}} \frac{|\langle n'l'j'm'_j, n''l''j''m''_j | V_{dd} | nljm_j, nljm_j \rangle|^2}{E_{n'l'j'm'_j} + E_{n''l''j''m''_j} - 2E_{nljm_j}}. \quad (3.16)$$

Equation (3.16) is the revised version of Eq. (3.12). When one of the energy denominators is small compared to the matrix element, one needs to use degenerate perturbation theory to find the level shift; this produces the revised version of Eq. (3.14). The level shifts for many different $|nljm_j, nljm_j\rangle$ have been calculated in Ref. [71]. Note that V can be positive or negative, depending on the state.

Even with all contributions included, the scaling forms in Eqs. (3.13) and (3.15) still hold [73]. For typical distances R in current experimental setups, the interaction is usually in the van der Waals regime. However, for special $|nljm_j, nljm_j\rangle$ states, an energy denominator in Eq. (3.16) almost vanishes, leading to the dipolar type of interaction. This is known as a Förster resonance, and the level shift is especially large. One can also apply a weak electric field to make an energy denominator vanish and thus obtain a Förster resonance.

In general, the level shifts are anisotropic. More precisely, the level shift depends on the angle between \hat{R} and the quantization axis, where \hat{R} points from one atom to the other. However, it turns out that the nS states are almost perfectly isotropic, due to the spherical symmetry of the S wavefunction [71]. As a result, the nS states are particularly useful in experiments.

3.4 Interaction in presence of a static electric field

In this section, we consider what happens when a static electric field is applied. We first describe how the energy levels of hydrogen are affected. Then we describe the dipole-dipole interaction between two hydrogen atoms. Finally, we discuss modifications when the atom is not hydrogen.

3.4.1 Single hydrogen atom

The Hamiltonian for the hydrogen atom in the absence of fine structure is

$$H_0 = \frac{p^2}{2m} - \frac{1}{4\pi\epsilon_0 r}. \quad (3.17)$$

A state is described by three quantum numbers, $|nlm\rangle$. Let the quantization axis be along \hat{z} , so m is the projection of l along \hat{z} . For a given n , all the lm states are degenerate. Now we turn on a weak electric field in the \hat{z} direction with amplitude ϵ , which adds a perturbation to the Hamiltonian,

$$H = H_0 + e\epsilon z. \quad (3.18)$$

The perturbation lifts the degeneracy among the lm states of a given n , leading to a first-order Stark shift. To see this, consider matrix elements between the original eigenstates: $\langle nl'm'|z|nlm\rangle$. Due to the dipole selection rules, the matrix element is nonzero only if $l' = l \pm 1$ and $m' = m$ [78]. Thus for a given n and m , multiple values of l are coupled together. The eigenstates of H are mixtures of lm states that

are coupled by the perturbation. Since the degeneracy is lifted in first order, the eigenvalues are linear in ε .

For example, consider $n = 3$. The groups of coupled states are: $\{|300\rangle, |310\rangle, |320\rangle\}$, $\{|31-1\rangle, |32-1\rangle\}$, $\{|311\rangle, |321\rangle\}$, $\{|32-2\rangle\}$, and $\{|322\rangle\}$. The states within each group mix to form the new eigenstates.

Since different values of l mix together, l is no longer a good quantum number. Instead, we use the parabolic quantum number q , which can take the values: $n - 1 - |m|, n - 3 - |m|, \dots, -(n - 1 - |m|)$ [26]. A Stark state is specified by $|nqm\rangle$. Note that m is still a good quantum number. The energy levels are [38]

$$E_{nqm} = \frac{3nqea_0\varepsilon}{2}, \quad (3.19)$$

where a_0 is the Bohr radius. As ε increases, the energy levels of a given n manifold increase and decrease linearly, since q can take on different values. This is called a first-order Stark shift. Since the Stark states are not parity eigenstates, they have permanent dipole moments,

$$\vec{\mu}_{nqm} = \frac{3nqea_0\hat{z}}{2}, \quad (3.20)$$

which are independent of the field strength ε .

3.4.2 Interaction of two hydrogen atoms

Now we consider the dipole-dipole interaction between two atoms in the presence of a static field. Suppose the atoms are in the two-atom state $|nqm, nqm\rangle$, where both atoms are in the same Stark state. Since Stark states have permanent dipole moments $\vec{\mu}$, the interaction is the same as between two classical dipoles. Equation (3.9) can be rewritten as

$$V_{dd} = \frac{1}{4\pi\epsilon_0 R^3} [\vec{\mu}_1 \cdot \vec{\mu}_2 - 3(\vec{\mu}_1 \cdot \hat{R})(\vec{\mu}_2 \cdot \hat{R})]. \quad (3.21)$$

The interaction is anisotropic, since it depends on the relative orientation between \hat{R} and the electric field. Suppose \hat{R} is perpendicular to the electric field. Then the two-atom state experiences a level shift,

$$V = \langle nqm, nqm | V_{dd} | nqm, nqm \rangle \quad (3.22)$$

$$= \frac{9(nqea_0)^2}{16\pi\epsilon_0 R^3}. \quad (3.23)$$

For example, consider the state with $q = n - 1$ and $m = 0$. This state has the largest Stark shift within a given n manifold. For large n , $V \sim n^4/R^3$.

3.4.3 Nonhydrogenic atoms

As discussed in Section 3.1, the nonhydrogenic atoms have a finite core size, and their energy levels are shifted by an amount that depends on l . Thus, for a given n , the lm states are not degenerate like they are in hydrogen. The $l \geq 3$ states can

still be considered degenerate, since their quantum defects are small. However, the $l = 0, 1, 2$ states are especially affected, since their quantum defects are large. The lack of degeneracy means that the $l = 0, 1, 2$ states have second-order Stark shifts, which are smaller than the usual first-order Stark shifts. But when the electric field is large enough to mix those states with others, the Stark shift becomes first-order [26]. Since it is complicated to accurately determine the energies and wavefunctions of nonhydrogenic atoms, it is common to use the hydrogen case as a rough estimate.

3.5 Rydberg blockade

Sections 3.3 and 3.4 showed that when two atoms are both in a Rydberg state, the dipole-dipole interaction leads to a level shift of the two-atom state. Here, we describe how the level shift affects the dynamics when the atoms are excited by a laser.

Let the ground state and a Rydberg state be denoted by $|g\rangle_i$ and $|r\rangle_i$, where i denotes which atom. $|r\rangle$ is shorthand for a particular Rydberg state ($|nljm_j\rangle$ or $|nqm\rangle$). The interaction term in the Hamiltonian is $V|r\rangle\langle r|_1 \otimes |r\rangle\langle r|_2$, which reflects the fact that when both atoms are in the Rydberg state, there is a level shift V . In principle, there is also a dipole-dipole interaction between the ground states, but it is much weaker than the Rydberg interaction, so we ignore it.

Suppose a laser shines on both atoms. The Hamiltonian is:

$$H = \sum_i \left[-\Delta|r\rangle\langle r|_i + \frac{\Omega}{2}(|g\rangle\langle r|_i + |r\rangle\langle g|_i) \right] + V|r\rangle\langle r|_1 \otimes |r\rangle\langle r|_2, \quad (3.24)$$

where Δ is the laser detuning and Ω is the Rabi frequency. Suppose the laser is on resonance ($\Delta = 0$). The system gets excited from $|gg\rangle$ to $|gr\rangle$ and $|rg\rangle$. However, due to the level shift, $|rr\rangle$ is shifted off resonance, so that it is effectively uncoupled from the other levels (Fig. 3.1(a)). Thus, the system stays within the space spanned by $\{|gg\rangle, |gr\rangle, |rg\rangle\}$. This is called *Rydberg blockade*, since the dipole-dipole interaction prevents the atoms from both being in the Rydberg state at the same time [57].

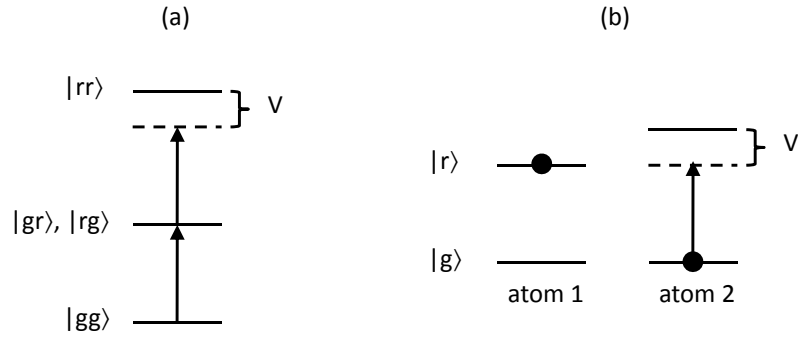


Figure 3.1: Two views of Rydberg blockade

In general, the dipole-dipole interaction leads to entanglement between the atoms. In fact, the blockade effect can be used to prepare entangled states, as seen in the following argument [57]. Let us work in the basis $\{|gg\rangle, |s\rangle, |a\rangle, |rr\rangle\}$, where $|s\rangle = (|gr\rangle + |rg\rangle)/\sqrt{2}$ and $|a\rangle = (|gr\rangle - |rg\rangle)/\sqrt{2}$. Due to the symmetry of H , the antisymmetric state $|a\rangle$ is uncoupled from the other states. Consider how the state $|\psi(t)\rangle = c_1(t)|gg\rangle + c_2(t)|s\rangle + c_3(t)|rr\rangle$ evolves under the Hamiltonian in Eq. (3.24):

$$i\dot{c}_1 = \frac{\Omega}{\sqrt{2}}c_2 \quad (3.25)$$

$$i\dot{c}_2 = \frac{\Omega}{\sqrt{2}}c_1 + \frac{\Omega}{\sqrt{2}}c_3 \quad (3.26)$$

$$i\dot{c}_3 = \frac{\Omega}{\sqrt{2}}c_2 + Vc_3. \quad (3.27)$$

Suppose both atoms start in the ground state: $c_1(0) = 1, c_2(0) = 0, c_3(0) = 0$. If V is very large, then $c_3(t) \approx 0$ for all times due to the blockade effect. Then Eqs. (3.25) and (3.26) become

$$i\dot{c}_1 = \frac{\Omega}{\sqrt{2}}c_2 \quad (3.28)$$

$$i\dot{c}_2 = \frac{\Omega}{\sqrt{2}}c_1. \quad (3.29)$$

At time $t = \pi/(\sqrt{2}\Omega)$, $c_1(t) = 0$ and $c_2(t) = 1$, which means that the atoms are in the entangled state $|s\rangle$. This scheme can be extended to entangle N atoms. Note that if $V = 0$, the atoms would never be entangled.

Here is another way of viewing the blockade effect. Again set $\Delta = 0$. Let atom 2 start in $|g\rangle$, and suppose the laser shines only on atom 2. If atom 1 is in $|g\rangle$, atom 2 gets excited to $|r\rangle$. However, if atom 1 is in $|r\rangle$, atom 2's Rydberg level is effectively shifted by V , so atom 2 is no longer on resonance with the laser and it stays in $|g\rangle$ (Fig. 3.1(b)). Thus, whether or not atom 2 gets excited to the Rydberg state depends on whether atom 1 is in the ground or Rydberg state.

Rydberg atoms have drawn much interest in the past decade because the blockade effect can be used for quantum information processing [57, 73] and many-body physics [66, 52, 33]. The rest of this thesis will be about how the Rydberg interaction can be used to study nonequilibrium physics.

Chapter 4

Antiferromagnetic phase transition in a nonequilibrium lattice of Rydberg atoms

In this chapter, we study a driven-dissipative system of atoms in the presence of laser excitation to a Rydberg state and spontaneous emission back to the ground state. The atoms interact via the blockade effect, whereby an atom in the Rydberg state shifts the Rydberg level of neighboring atoms. We use mean-field theory to study how the Rydberg population varies in space. As the laser frequency changes, there is a continuous transition between the uniform and antiferromagnetic phases. The nonequilibrium nature also leads to a novel oscillatory phase and bistability between the uniform and antiferromagnetic phases. The results of this chapter were published in Ref. [47].

4.1 Model

We briefly review the Rydberg interaction, which was described in Chapter 3. Suppose two atoms are in the same Rydberg state nlj . There is a dipole-dipole matrix element

between $|nlj, nlj\rangle$ and nearby energy levels, and this interaction shifts the energy of $|nlj, nlj\rangle$ by an amount V . When the atoms are separated by a small distance R , the dipolar interaction dominates ($V \approx -C_3/R^3$), but for large distances, the van der Waals interaction dominates ($V \approx -C_6/R^6$). For mathematical convenience, we use the van der Waals interaction and a $|ns_{1/2}, ns_{1/2}\rangle$ state, so that the interaction is short range and isotropic. However, it is straightforward to extend the analysis to long-range and anisotropic interactions.

Consider a lattice of atoms that is uniformly excited by a laser from the ground state to a Rydberg state. The atoms are assumed to be fixed in space. Since the van der Waals interaction decreases rapidly with distance, we assume nearest-neighbor interactions. Let $|g\rangle_j$ and $|e\rangle_j$ denote the ground and Rydberg states of atom j . The Hamiltonian in the interaction picture and rotating-wave approximation is ($\hbar = 1$)

$$H = \sum_j H_j + V \sum_{\langle jk \rangle} |e\rangle\langle e|_j \otimes |e\rangle\langle e|_k, \quad (4.1)$$

$$H_j = -\tilde{\Delta} |e\rangle\langle e|_j + \frac{\tilde{\Omega}}{2} (|e\rangle\langle g|_j + |g\rangle\langle e|_j). \quad (4.2)$$

The second term in Eq. (4.1) is the Rydberg interaction, and H_j is the Hamiltonian for a two-level atom interacting with a laser. $\tilde{\Delta} = \omega_\ell - \omega_o$ is the detuning between the laser and transition frequencies. $\tilde{\Omega}$ is the Rabi frequency, which depends on the laser intensity.

The lifetime of the Rydberg state is limited by several processes: spontaneous emission, blackbody radiation, and superradiance. We account for spontaneous emis-

sion from the Rydberg level using the linewidth γ . When a Rydberg atom spontaneously decays, it usually goes directly into the ground state or, first, to a low-lying state [19]; the low-lying states are relatively short-lived, so we ignore them. We also ignore blackbody radiation and superradiance¹, both of which transfer atoms in a Rydberg level to nearby levels. Blackbody radiation can be minimized by working at cryogenic temperatures [10], and it is not clear if superradiance is important when the interaction V is large [89, 19]. Future treatments could account for them by considering several Rydberg levels instead of just one.

Thus, each atom has two possible states, and the system is equivalent to a dissipative spin model. Previous works have added dissipation to other spin models by coupling each spin to a heat bath; in those works, there is global thermal equilibrium, and the spins are described by an effective partition function [91, 80]. However, in quantum optics, dissipation from spontaneous emission leads to a nonequilibrium situation, since the coupling to the heat bath is weak and Markovian [14]. The density matrix for the atoms, ρ , is described by a master equation that is local in time:

$$\dot{\rho} = -i[H, \rho] + \gamma \sum_j \left(-\frac{1}{2} \{ |e\rangle\langle e|_j, \rho \} + |g\rangle\langle e|_j \rho |e\rangle\langle g|_j \right). \quad (4.3)$$

The nonequilibrium nature is exhibited in the interplay between unitary and dissipative dynamics [21, 83], and we are interested in the properties of the steady-state

¹Superradiance is a cooperative phenomenon that affects the radiative decay of a group of atoms [29]. When the distance between atoms is smaller than the wavelength of the atomic transition, the atoms are coupled to the same electromagnetic modes. Due to quantum effects, the spontaneous emission rate is enhanced compared to a single atom. For Rydberg atoms, superradiance can be important, since transitions between Rydberg states have long wavelengths. In fact, superradiance was observed with Rydberg atoms in Ref. [70].

solution of Eq. (4.3).

4.2 Mean-field theory

Due to the complexity of the full quantum problem, we use mean-field theory. For equilibrium spin models, mean-field theory is useful for determining the existence of different phases [4]. Its predictions are accurate in high dimensions but not in low dimensions. For the current nonequilibrium case, we use the approach of Refs. [21, 83]: factorize the density matrix by site, $\rho = \bigotimes_j \rho_j$, and work with the reduced density matrices, $\rho_j = \text{Tr}_{\neq j} \rho$. This accounts for on-site quantum fluctuations but not inter-site fluctuations: for atom j , the interaction, $|e\rangle\langle e|_j \otimes \sum_k |e\rangle\langle e|_k$, is replaced with the mean field, $|e\rangle\langle e|_j \sum_k \rho_{k,ee}$. In high dimensions, this is a good approximation, since fluctuations of the neighbors average out.

Then the evolution of each ρ_j is given by

$$\dot{w}_j = -2\tilde{\Omega} \text{Im } q_j - \gamma(w_j + 1), \quad (4.4)$$

$$\dot{q}_j = i \left[\tilde{\Delta} - \frac{V}{2} \sum_{\langle jk \rangle} (w_k + 1) \right] q_j - \frac{\gamma}{2} q_j + i \frac{\tilde{\Omega}}{2} w_j, \quad (4.5)$$

where we have defined the inversion $w_j \equiv \rho_{j,ee} - \rho_{j,gg}$ and off-diagonal element $q_j \equiv \rho_{j,eg}$. The Rydberg population $\rho_{j,ee} = (w_j + 1)/2$ is the observable measured in the experiment by measuring the photon scattering rate of each atom. $w_j = -1$ and 1 mean that the atom is in the ground and Rydberg states, respectively. Equations (4.4) and (4.5) are the optical Bloch equations, except that the Rydberg interaction

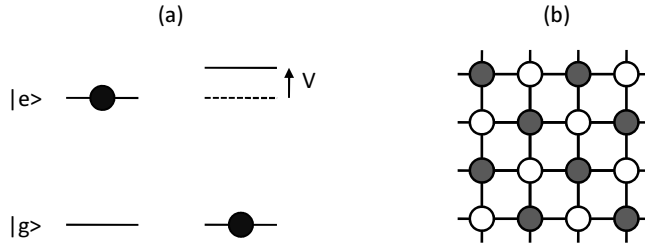


Figure 4.1: (a) When one atom is excited to the Rydberg state, it shifts the transition frequency of a neighboring atom by V . (b) The lattice is divided into two sublattices.

introduces nonlinearity: the detuning for an atom is renormalized by the excitation of its neighbors (Fig. 4.1(a)).

Since the system is dissipative, it will end up at an attracting solution, which can be a fixed point, limit cycle, quasiperiodic orbit, or strange attractor [82]. (We have not observed the latter two.) We want to know: for given parameter values, how many steady-state solutions are there and are they stable? A solution is stable or unstable if a perturbation to it decays or grows, respectively; the system will end up only in a stable solution.

Equations (4.4) and (4.5) always have a steady-state solution, in which the Rydberg population is uniform across the lattice ($w_j = w$, $q_j = q$). For some parameter values, this uniform solution is stable, but for others, it is unstable to perturbations of wavelength 2. In the latter case, the lattice divides into two alternating sublattices, and the atoms on one sublattice have higher Rydberg population than the other (Fig. 4.1(b)). Hence an antiferromagnetic pattern emerges from the uniform solution through a dynamical instability. To simplify the discussion here, we keep track of only the two sublattices instead of every site. We stress that the antiferromagnetic transition is not an artifact of dividing the lattice into two sublattices, as shown

explicitly in Appendix 4.B.

To simplify the equations, we rescale time by γ and also rescale the Rabi frequency $\Omega = \tilde{\Omega}/\gamma$, detuning $\Delta = \tilde{\Delta}/\gamma$, and interaction $c = dV/\gamma = -dC_6/\gamma R^6$, where d is the lattice dimension. Labeling the sublattices 1 and 2,

$$\dot{w}_1 = -2\Omega \operatorname{Im} q_1 - w_1 - 1, \quad (4.6)$$

$$\dot{w}_2 = -2\Omega \operatorname{Im} q_2 - w_2 - 1, \quad (4.7)$$

$$\dot{q}_1 = i[\Delta - c(w_2 + 1)]q_1 - \frac{q_1}{2} + i\frac{\Omega}{2}w_1, \quad (4.8)$$

$$\dot{q}_2 = i[\Delta - c(w_1 + 1)]q_2 - \frac{q_2}{2} + i\frac{\Omega}{2}w_2. \quad (4.9)$$

There are six nonlinear differential equations (since q_1 and q_2 are complex) and three parameters (Ω , Δ , c). The uniform version of these equations ($w_1 = w_2$, $q_1 = q_2$) has been studied before in the context of a medium that interacts with its own electromagnetic field; it is known that there is bistability [34]. We are considering the more general case by letting the sublattices differ.

4.3 Mean-field results

In Appendix 4.A, we determine the solutions and stabilities for Eqs. (4.6)–(4.9). Here, we summarize the main results. Consider first the fixed points, i.e., when $\dot{w}_1 = \dot{w}_2 = \dot{q}_1 = \dot{q}_2 = 0$. There are two types of fixed points: the uniform fixed points ($w_1 = w_2$) correspond to spatially homogeneous Rydberg excitation, while the nonuniform fixed points ($w_1 \neq w_2$) correspond to the antiferromagnetic phase, i.e.,

when one sublattice has higher excitation than the other.

There are either one or three uniform fixed points, corresponding to the real roots of a cubic polynomial,

$$f(w) = c^2 w^3 - c(2\Delta - 3c)w^2 + \left[\frac{\Omega^2}{2} + \frac{1}{4} + (\Delta - 3c)(\Delta - c) \right] w + (\Delta - c)^2 + \frac{1}{4}. \quad (4.10)$$

As the parameters change, pairs of uniform fixed points appear and disappear via saddle-node bifurcations. The uniform fixed points never undergo Hopf bifurcations, so we do not expect limit cycles emerging from them [82].

There are up to two nonuniform fixed points, given by the real roots of a quadratic polynomial,

$$g(w) = c^2(1 + 4\Delta^2 + 2\Omega^2)w^2 - 2c[(\Delta - c)(1 + 4\Delta^2) + (2\Delta - c)\Omega^2]w + c^2(1 + 4\Delta^2) - 2c\Delta(1 + 4\Delta^2 + 2\Omega^2) + \frac{1}{4}(1 + 4\Delta^2 + 2\Omega^2)^2. \quad (4.11)$$

The two roots correspond to w_1 and w_2 . As the parameters change, the two nonuniform fixed points appear and disappear together.

Since the laser detuning Δ is the easiest parameter to vary experimentally, we describe what happens as a function of it (Fig. 4.2). Suppose Δ starts out large and negative. There is one stable uniform fixed point and no other fixed points. As Δ increases, the uniform fixed point may undergo a pitchfork bifurcation, in which it becomes unstable and the nonuniform fixed points appear. The bifurcation is

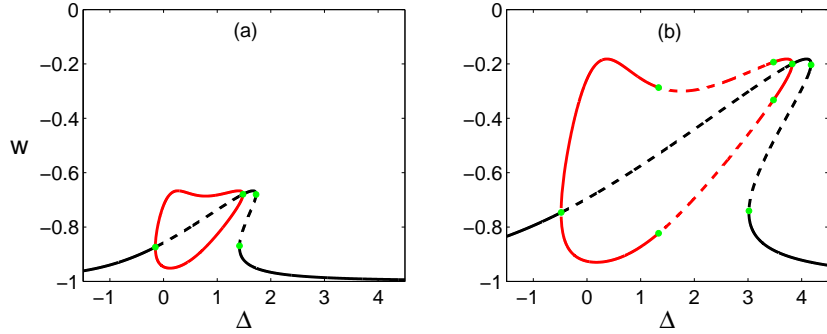


Figure 4.2: Bifurcation diagram showing fixed-point solutions as function of Δ , with $c = 5$ and (a) $\Omega = 0.5$ and (b) $\Omega = 1.5$. The inversion w is -1 (1) when the atom is in the ground (Rydberg) state. Solid (dashed) lines denote stable (unstable) fixed points. Black (red) lines denote uniform (nonuniform) fixed points. Green points denote bifurcations. In (b), the nonuniform fixed points undergo Hopf bifurcations at $\Delta = 3.48$ and 1.33 , and there is a stable limit cycle in that interval [shown in Fig. 4.3(a)].

supercritical, which means that when the nonuniform fixed points appear, they are stable and coincide with the uniform fixed point [82]. Thus, this is a continuous phase transition between the uniform and antiferromagnetic phases. As Δ increases further, there is another supercritical pitchfork bifurcation, in which the same uniform fixed point becomes stable again and the nonuniform fixed points disappear. As Δ increases further towards ∞ , there is again one stable uniform fixed point and no other fixed points.

Although the nonuniform fixed points are stable when they appear and disappear, they could become unstable in between via a Hopf bifurcation [82]. We find numerically that sometimes the nonuniform fixed points do have Hopf bifurcations (Fig. 4.2(b)) and give rise to a stable limit cycle, in which w_1 and w_2 oscillate periodically in time (Fig. 4.3(a)). This oscillatory phase is due to the nonequilibrium nature of the system.

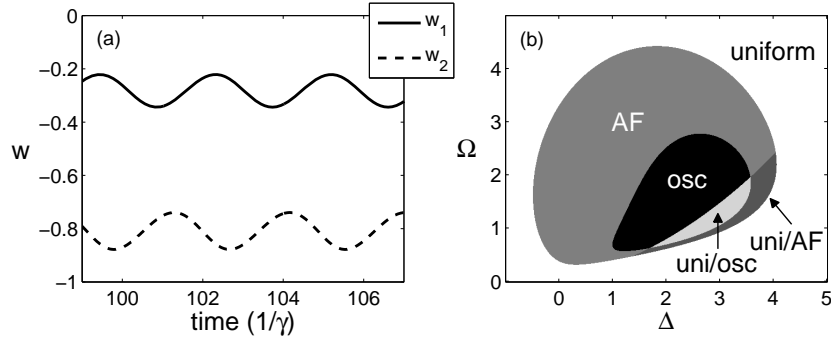


Figure 4.3: (a) Oscillatory steady-state solution (limit cycle) for $c = 5$, $\Omega = 1.5$, and $\Delta = 1.5$. (b) Phase diagram for mean-field theory in Ω, Δ space for $c = 5$. The system is either in the uniform, antiferromagnetic, or oscillatory phase. It can be bistable between uniform and antiferromagnetic phases or between uniform and oscillatory phases.

Thus, in mean-field theory, there are three phases: uniform, antiferromagnetic, and oscillatory. Figure 4.3(b) shows a phase diagram in Δ, Ω space. For some parameters, the system is bistable between uniform and antiferromagnetic or between uniform and oscillatory (Fig. 4.2(b)); the final state depends on the initial conditions.

The existence of the antiferromagnetic phase can be intuitively understood from the fact that the effective detunings for sublattices 1 and 2 are $\Delta_1 = \Delta - c(w_2 + 1)$ and $\Delta_2 = \Delta - c(w_1 + 1)$, respectively (Eqs. (4.8)–(4.9)). Suppose the atoms are originally on resonance ($\Delta \approx 0$) and sublattice 1 is excited ($w_1 \approx 0$). This shifts sublattice 2 off resonance ($\Delta_2 \approx -c$), so it is in the ground state ($w_2 \approx -1$). Then sublattice 1 remains on resonance ($\Delta_1 \approx 0$), so it remains excited ($w_1 \approx 0$). Thus the antiferromagnetic phase arises from the nonequilibrium properties of the system, in contrast to equilibrium systems, where it is due to the balance of energy and entropy [4]. However, the critical exponent β is the same as the equilibrium mean-field value. Near the pitchfork bifurcation ($\Delta \approx \Delta_c$), the nonuniform fixed points

satisfy $w(\Delta - \Delta_c) - w(\Delta_c) \sim \pm|\Delta - \Delta_c|^{1/2}$, so $\beta = 1/2$.

4.4 Original quantum model

Since mean-field theory is an approximation, we also numerically solve the original master equation, Eq. (4.3), in 1D, where mean-field theory is least accurate. We use fourth-order Runge-Kutta integration to find the steady state ρ for a chain of length $N = 10$. Figure 4.4(a) shows the correlation as a function of distance, $\langle E_i E_{i+j} \rangle - \langle E_i \rangle \langle E_{i+j} \rangle$, where $E_i = |e\rangle\langle e|_i$. The rapid decay suggests that there is no long-range order in 1D, but the fact that it alternates sign means that there is an antiferromagnetic tendency. We also calculate the order parameter, $[\langle (E_e - E_o)^2 \rangle]^{1/2}$, where the operator $E_e = \frac{2}{N} \sum_{i \text{ even}} E_i$ measures the average Rydberg population on the even sublattice, and E_o does likewise for the odd sublattice. The order parameter measures the difference between the two sublattices: it is 0 when they are identical (uniform phase), but positive when they are different (antiferromagnetic and oscillatory phases). The order parameter is largest for roughly the same parameter space, for which mean-field theory predicts the uniform phase to be unstable (compare Fig. 4.4(b) with Fig. 4.2(b)). Thus, mean-field theory captures some qualitative aspects of the full quantum model in 1D, but it remains to be seen whether there is long-range order in higher dimensions, where mean-field theory is more accurate. Chapter 5 investigates the original quantum model in the regime where mean-field theory predicts bistability of uniform fixed points.

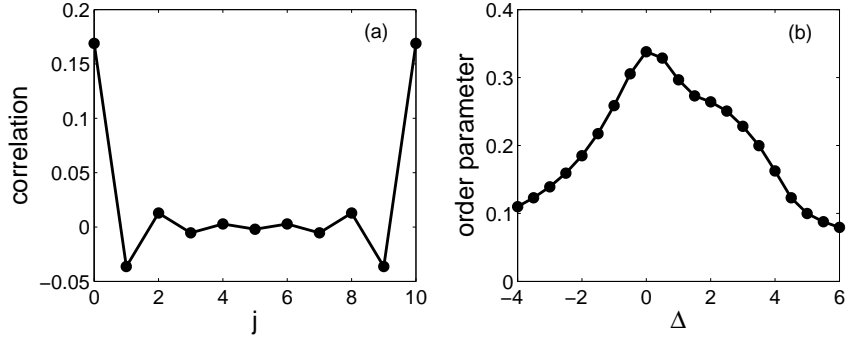


Figure 4.4: Numerical solution of master equation for 1D chain of length $N = 10$ with periodic boundary conditions. Steady state ρ is found after integrating for time $\gamma t = 20$. Parameters are $\Omega = 1.5$ and $V = 5\gamma$, which is equivalent to Fig. 4.2(b). (a) Correlation as a function of distance j for $\Delta = 0$. (b) Order parameter as a function of detuning

4.5 Experimental considerations

Since it is difficult to simulate large systems, experiments with atoms in an optical lattice could provide much information. For example, one can use ^{87}Rb and a two-photon excitation scheme to go from the ground state $5s_{1/2}$ to the Rydberg state $23s_{1/2}$, which has van der Waals interaction $C_6 = -870 \text{ kHz } \mu\text{m}^6$ [71] and linewidth $\gamma/2\pi = 14.7 \text{ kHz}$ at 0 K [10]. A d -dimensional lattice with spacing $R = 1.5 \mu\text{m}$ has interaction strength $V = 76 \text{ kHz}$ and $c = 5.2d$. The Rydberg population of each atom may be measured by imaging the spontaneously emitted photons; in the antiferromagnetic phase, every other atom fluoresces more. Alternatively, the ground-state population may be measured using repeated projective measurements on a $5s - 5p$ transition. A practical setup would be to use a microscope that both produces the lattice and images the atoms [7].

To have the same trap potential for ground and Rydberg states, both states should have the same polarizability, so the lattice light should be blue-detuned with respect

to the $5s - 5p$ transitions [73]. This would also minimize the photoionization induced by lattice light, since the atoms would sit at the minimum of the light intensity. A practical setup would be to use a microscope that both produces the lattice and images the atoms [7]; this allows the lattice spacing to be independent of the wavelength of the lattice light.

4.6 Conclusion

Thus, a driven-dissipative system of Rydberg atoms has a unique type of antiferromagnetism. The next step is to investigate in more detail how the full quantum model behaves in low dimensions. The existence of limit cycles in the mean-field limit is particularly surprising, and it would be interesting to see what happens to them in low dimensions. Limit cycles occur in the mean-field limit of other models, such as cavity QED [3], second-harmonic generation [22], and optomechanics [58]. In those models, a limit cycle means that the number of photons in an optical cavity oscillates in time. As the system becomes more quantum, the limit cycles still exist, but quantum fluctuations cause the oscillations to become noisy.

Our work can be extended to Rydberg states with anisotropic and long-range interactions. Such interactions usually give rise to very rich physics [44], so the nonequilibrium version should be interesting. One can also see what happens when the atoms are not fixed on a lattice but free to move; this is reminiscent of classical reaction-diffusion systems [17, 16]. Finally, we note that a system of interacting Rydberg atoms is similar to a system of spins interacting with each other's magnetic

dipolar field [39, 55]. Thus, when an NMR system is made nonequilibrium with continuous driving and spin relaxation, the spins may form a stable pattern in space.

4.A Mean-field solutions for sublattices

This appendix provides details on the steady-state solutions of the mean-field model, where we only keep track of the two sublattices. One might wonder whether the antiferromagnetic phase is an artifact of dividing up the lattice into two sublattices. Appendix 4.B discusses the mean-field solutions without assuming sublattices and shows that the antiferromagnetic phase is not an artifact.

Let the two sublattices be labelled 1 and 2. The system is described by

$$\dot{w}_1 = -2\Omega \operatorname{Im} q_1 - w_1 - 1, \quad (4.12)$$

$$\dot{w}_2 = -2\Omega \operatorname{Im} q_2 - w_2 - 1, \quad (4.13)$$

$$\dot{q}_1 = i [\Delta - c(w_2 + 1)] q_1 - \frac{q_1}{2} + i \frac{\Omega}{2} w_1, \quad (4.14)$$

$$\dot{q}_2 = i [\Delta - c(w_1 + 1)] q_2 - \frac{q_2}{2} + i \frac{\Omega}{2} w_2. \quad (4.15)$$

Remember that w_1, w_2 are real while q_1, q_2 are complex. There are six differential equations and three parameters (Ω, Δ, c) . The equations are symmetric under the transformations $\{w_1, q_1 \leftrightarrow w_2, q_2\}$, $\{\Delta, c, q_1, q_2 \rightarrow -\Delta, -c, -q_1^*, -q_2^*\}$, and $\{\Omega, q_1, q_2 \rightarrow -\Omega, -q_1, -q_2\}$.

We focus on the fixed points of the system, i.e., when $\dot{w}_1 = \dot{w}_2 = \dot{q}_1 = \dot{q}_2 = 0$.

The fixed points are given by the simultaneous roots of two cubic polynomials:

$$f_1(w_1, w_2) = (w_1 + 1) \left\{ \frac{1}{4} + [\Delta - c(w_2 + 1)]^2 \right\} + \frac{\Omega^2}{2} w_1, \quad (4.16)$$

$$f_2(w_1, w_2) = (w_2 + 1) \left\{ \frac{1}{4} + [\Delta - c(w_1 + 1)]^2 \right\} + \frac{\Omega^2}{2} w_2. \quad (4.17)$$

Once w_1 and w_2 are found, q_1 and q_2 can be calculated,

$$q_1(w_1, w_2) = \frac{-\frac{\Omega}{2} w_1 [\Delta - c(w_2 + 1)] + i \frac{\Omega}{4} w_1}{\frac{1}{4} + [\Delta - c(w_2 + 1)]^2}, \quad (4.18)$$

$$q_2(w_1, w_2) = \frac{-\frac{\Omega}{2} w_2 [\Delta - c(w_1 + 1)] + i \frac{\Omega}{4} w_2}{\frac{1}{4} + [\Delta - c(w_1 + 1)]^2}. \quad (4.19)$$

Since $f_1(w_1 \leq -1, w_2)$ is negative and $f_1(w_1 \geq 0, w_2)$ is positive (and similarly for f_2 and w_2), we know that the fixed points lie in the range $w_1, w_2 \in [-1, 0]$.

By combining f_1 and f_2 , we find that the fixed points correspond to the real roots of a fifth-order polynomial $h(w)$, which is too complicated to show here. Fortunately, one can factor it. Note that there are two kinds of fixed points: a uniform fixed point ($w_1 = w_2$ and $q_1 = q_2$) means that the two sublattices are identical, and a nonuniform fixed point ($w_1 \neq w_2$ and $q_1 \neq q_2$) means that the system is in the antiferromagnetic phase. The uniform fixed points are given by real roots of a cubic polynomial, $f(w) = f_1(w, w)$,

$$f(w) = c^2 w^3 - c(2\Delta - 3c)w^2 + \left[\frac{\Omega^2}{2} + \frac{1}{4} + (\Delta - 3c)(\Delta - c) \right] w + (\Delta - c)^2 + \frac{1}{4}. \quad (4.20)$$

Since the roots of f are also roots of h , we know that f is a factor of h . Thus, $h(w) = 4f(w)g(w)$ and the real roots of the quadratic polynomial $g(w)$ correspond to nonuniform fixed points,

$$g(w) = c^2(1 + 4\Delta^2 + 2\Omega^2)w^2 - 2c[(\Delta - c)(1 + 4\Delta^2) + (2\Delta - c)\Omega^2]w + c^2(1 + 4\Delta^2) - 2c\Delta(1 + 4\Delta^2 + 2\Omega^2) + \frac{1}{4}(1 + 4\Delta^2 + 2\Omega^2)^2. \quad (4.21)$$

Hence, there are at most three uniform fixed points and two nonuniform fixed points. One should think of the two nonuniform fixed points as being a joint pair, since they correspond to w_1 and w_2 .

At this point, the uniform and nonuniform fixed points can be found by numerically solving for the roots of f and g , and their stabilities can be determined by calculating the eigenvalues of the Jacobian for each fixed point. However, to obtain general results, we derive as much information as possible analytically without explicitly solving for the fixed points. In particular, we care about the number of each kind of fixed point and their stabilities as a function of the parameters.

4.A.1 Number of uniform fixed points

Here, we examine the number of uniform fixed points, i.e., the number of real roots of $f(w)$. Since f is cubic, it has one or three real roots (two in special cases). Suppose c and Δ have opposite signs. The polynomial $\tilde{f}(\tilde{w}) \equiv f(w = \tilde{w} - 1)$ has coefficients with signs $+++ -$. By Descartes' rule of signs [6], $\tilde{f}(\tilde{w})$ has exactly one positive root, which means that $f(w)$ has exactly one root with $w > -1$. Since we know that

all roots of $f(w)$ are in the interval $[-1, 0]$, this shows that if c and Δ have opposite signs, there is only one root.

Now we check when f has three roots. Since f is cubic, it has three roots when the local maximum and minimum exist and are positive and negative, respectively. Thus, there are three roots if and only if

$$4\Delta^2 > 6\Omega^2 + 3 \quad \text{and} \quad (4.22)$$

$$c \in \left(\frac{2\Delta(18\Omega^2 + 4\Delta^2 + 9) - (4\Delta^2 - 6\Omega^2 - 3)^{\frac{3}{2}}}{54\Omega^2}, \frac{2\Delta(18\Omega^2 + 4\Delta^2 + 9) + (4\Delta^2 - 6\Omega^2 - 3)^{\frac{3}{2}}}{54\Omega^2} \right). \quad (4.23)$$

According to this condition, for large $|\Delta|$, there is exactly one root, i.e., one uniform fixed point, regardless of the sign of c .

4.A.2 Stability of uniform fixed points

We check the linear stability of the uniform fixed points to perturbations. Since Eqs. (4.12)–(4.15) are symmetric between 1 and 2, the eigenvectors of the Jacobian for uniform fixed points are either symmetric or antisymmetric between 1 and 2. (The symmetric eigenvectors correspond to perturbations that affect 1 and 2 identically, while the antisymmetric eigenvectors represent perturbations that affect 1 and 2 in opposite directions.) This is convenient, because we can check the stability to symmetric and antisymmetric perturbations separately, and the characteristic polynomials are cubic instead of sixth degree. A uniform fixed point is stable overall if it

is stable to both kinds of perturbations.

The Routh-Hurwitz criterion is very useful here because it can provide stability information without explicitly knowing the fixed point [56]. Suppose the characteristic polynomial for a fixed point is cubic: $\lambda^3 + a_2\lambda^2 + a_1\lambda + a_0$. All the eigenvalues have a negative real part if and only if $a_2, a_0, a_1a_2 - a_0 > 0$; this means the fixed point is stable. All the eigenvalues have a negative real part, except for a pair of purely imaginary roots, if and only if $a_2, a_0 > 0$ and $a_2a_1 - a_0 = 0$; this indicates a Hopf bifurcation [82].

4.A.2.1 Stability to symmetric perturbations

First we consider the stability of a uniform fixed point to symmetric perturbations. In this case, we can consider a simpler system by letting $w \equiv w_1 = w_2$, $q \equiv q_1 = q_2$, and

$$\dot{w} = -2\Omega \operatorname{Im} q - w - 1, \quad (4.24)$$

$$\dot{q} = i[\Delta - c(w+1)]q - \frac{q}{2} + i\frac{\Omega}{2}w, \quad (4.25)$$

whose fixed points are given by the roots of $f(w)$ in Eq. (4.20). Once w is found, q is given by

$$q = \frac{-\frac{\Omega}{2}w[\Delta - c(w+1)] + i\frac{\Omega}{4}w}{\frac{1}{4} + [\Delta - c(w+1)]^2}. \quad (4.26)$$

The characteristic polynomial for a fixed point w, q is

$$\begin{aligned} \alpha(\lambda) = & \lambda^3 + 2\lambda^2 + \left\{ [\Delta - c(w+1)]^2 + \Omega^2 + \frac{5}{4} - 2\Omega c \operatorname{Re} q \right\} \lambda \\ & + [\Delta - c(w+1)]^2 + \frac{\Omega^2}{2} + \frac{1}{4} - 2\Omega c \operatorname{Re} q. \end{aligned} \quad (4.27)$$

For $\alpha(\lambda)$, we see that $a_2 > 0$ and $a_2 a_1 - a_0 = a_0 + \Omega^2 + 2$. According to the Routh-Hurwitz criterion given above, the fixed point is stable to symmetric perturbations if and only if $a_0 > 0$. Also, since $a_2 a_1 - a_0 > a_0$, there is never a Hopf bifurcation from symmetric perturbations for any uniform fixed point.

Now suppose c and Δ have opposite signs. We showed in Section 4.A.1 that in this case, there is one uniform fixed point. We also see that $2\Omega c \operatorname{Re} q \leq 0$ in this case and hence $a_0 > 0$. Thus the single uniform fixed point is stable to symmetric perturbations.

Since f is cubic, fixed points of Eqs. (4.24)–(4.25) appear and disappear through saddle-node bifurcations as the parameters change [82]. In a saddle-node bifurcation, two fixed points with opposite stabilities appear or disappear together. Also, since there is never a Hopf bifurcation, a given fixed point has the same stability as the parameters change.

These statements allow us to deduce the stabilities of all the uniform fixed points. Suppose we start with c and Δ having opposite signs. There is a single uniform fixed point and it is stable as shown above. As we change the parameters, eventually it collides with another uniform fixed point via a saddle-node bifurcation, so the second fixed point must be unstable. Furthermore, that unstable fixed point undergoes a

saddle-node bifurcation with a third fixed point, so the third fixed point must be stable, even when it is the only fixed point. (Remember that these stabilities are with respect to symmetric perturbations.)

To summarize, when there is one uniform fixed point, it is stable to symmetric perturbations. When there are three uniform fixed points, the outer two (highest and lowest values of w) are stable to symmetric perturbations, while the inner one (middle value of w) is unstable to symmetric perturbations. Of course, the outer fixed points could be unstable to antisymmetric perturbations, which is what we check in the next section.

4.A.2.2 Stability to antisymmetric perturbations

We now check when the uniform fixed points become unstable to antisymmetric perturbations. Let the fixed point be w, q . We consider antisymmetric perturbations around it: $w_1 = w + \delta w$, $w_2 = w - \delta w$, $q_1 = q + \delta q$, and $q_2 = q - \delta q$. By plugging into Eqs. (4.12)–(4.15) and linearizing for small $\delta w, \delta q$, we find the characteristic polynomial,

$$\begin{aligned} \beta(\lambda) = & \lambda^3 + 2\lambda^2 + \left\{ [\Delta - c(w+1)]^2 + \Omega^2 + \frac{5}{4} + 2\Omega c \operatorname{Re} q \right\} \lambda \\ & + [\Delta - c(w+1)]^2 + \frac{\Omega^2}{2} + \frac{1}{4} + 2\Omega c \operatorname{Re} q, \end{aligned} \quad (4.28)$$

which is similar to Eq. (4.27). For $\beta(\lambda)$, we see that $a_2 > 0$ and $a_2 a_1 - a_0 = a_0 + \Omega^2 + 2$.

According to the Routh-Hurwitz criterion given above, the fixed point is stable to

antisymmetric perturbations if and only if $a_0 > 0$, i.e.,

$$[\Delta - c(w + 1)]^2 + \frac{\Omega^2}{2} + \frac{1}{4} + 2\Omega c \operatorname{Re} q > 0. \quad (4.29)$$

We can simplify this using the fact that the fixed point satisfies $f(w) = 0$: the uniform fixed point is stable to antisymmetric perturbations if and only if

$$\phi(w) \equiv c^2 w^2 + 2c^2 w + c^2 - \Delta^2 - \frac{\Omega^2}{2} - \frac{1}{4} < 0. \quad (4.30)$$

So when a uniform fixed point is on the verge of instability, it satisfies

$$w = -1 + \frac{\sqrt{1 + 4\Delta^2 + 2\Omega^2}}{2|c|}. \quad (4.31)$$

For large $|\Delta|$, $\phi < 0$, so the one uniform fixed point that exists is stable to both symmetric and antisymmetric perturbations.

Note that since $a_2 a_1 - a_0 > a_0$, there is never a Hopf bifurcation from antisymmetric perturbations. Since we already ruled out Hopf bifurcations from symmetric perturbations, we conclude that uniform fixed points never have Hopf bifurcations.

4.A.3 Nonuniform fixed points

The nonuniform fixed points are given by the roots of the quadratic polynomial $g(w)$ in Eq. (4.21). The two nonuniform fixed points appear and disappear together as the parameters change. The symmetry in Eqs. (4.12)–(4.15) between 1 and 2 means

that the two nonuniform fixed points have the same stability. Thus, the nonuniform fixed points must appear via a pitchfork bifurcation from a uniform fixed point as the parameters change [82]. In other words, the nonuniform fixed points intersect with a uniform fixed point, which changes stability at the intersection. (In Section 4.A.4, we will determine whether the bifurcation is supercritical or subcritical and which uniform fixed point is involved.)

The intersection of the nonuniform fixed points with a uniform fixed point can be shown explicitly. From $g(w)$, the nonuniform fixed points exist if and only if $\zeta(\Omega, \Delta, c) < 0$, where

$$\begin{aligned} \zeta(\Omega, \Delta, c) = & 16(1 + 2\Omega^2)\Delta^4 - 32c\Omega^2\Delta^3 + 8(1 + 2\Omega^2)^2\Delta^2 \\ & - 8c\Omega^2(1 + 2\Omega^2)\Delta + (1 + 2\Omega^2)^3 - 4c^2\Omega^4. \end{aligned} \quad (4.32)$$

On the verge of the appearance of the nonuniform fixed points, $\zeta = 0$ and the root of $g(w)$ is

$$w = -1 + \frac{\Delta}{c} + \frac{\Omega^2}{1 + 4\Delta^2 + 2\Omega^2}. \quad (4.33)$$

One can show that Eqs. (4.31) and (4.33) are equal using $f(w) = 0$. Thus, the change in stability of a uniform fixed point coincides with the appearance of the nonuniform fixed points.

In the case when $|\Delta|$ is large, $\zeta \sim \Delta^4$, so nonuniform fixed points do not exist.

There is a convenient sufficient condition for the existence of the nonuniform fixed

points. If $\zeta(\Delta = 0) = (1 + 2\Omega^2)^3 - 4c^2\Omega^4 < 0$, there is a range of Δ around $\Delta = 0$, for which the nonuniform fixed points exist. In other words, if

$$|c| > \frac{(2\Omega^2 + 1)^{\frac{3}{2}}}{2\Omega^2}, \quad (4.34)$$

there is a range of Δ around $\Delta = 0$, for which nonuniform fixed points exist.

4.A.4 Connection between uniform and nonuniform fixed points

We describe what happens as Δ changes. Without loss of generality (due to symmetry), assume $c > 0$. Suppose Δ starts out large and negative. There is one uniform fixed point and it is stable. Nonuniform fixed points do not exist. Then let Δ increase. At some point, a uniform fixed point may undergo a pitchfork bifurcation: it becomes unstable to antisymmetric perturbations and the nonuniform fixed points appear. The fact that the nonuniform fixed points exist when the uniform fixed point is unstable indicates that the bifurcation is supercritical [82].

When the pitchfork bifurcation happens, there may be three uniform fixed points. Which one undergoes the bifurcation? Since $\phi(w) \sim w^2$ in Eq. (4.30), as Δ decreases, the first uniform fixed point to go unstable must be the upper one (the one with the highest w). Furthermore, since there can be at most two nonuniform fixed points, only the upper uniform fixed point may be unstable to antisymmetric perturbations. We conclude that when there are three uniform fixed points, only the upper one may undergo a pitchfork bifurcation, and the lower one is stable. According to Section 4.A.2.1, the middle uniform fixed point is always unstable.

It is possible that the pitchfork bifurcation happens when there is only one uniform fixed point. Then obviously that fixed point must undergo the pitchfork bifurcation.

Since the pitchfork bifurcation is supercritical, the nonuniform fixed points are stable when they appear.

Then let Δ increase towards ∞ . Eventually $\zeta > 0$ and $\phi < 0$ again. This indicates that there was another pitchfork bifurcation in which the nonuniform fixed points disappeared and the uniform fixed point became stable again.

Note that we have not determined here whether the nonuniform fixed points ever have Hopf bifurcations. As stated in Section 4.3, we found numerically that they do sometimes have Hopf bifurcations.

4.B Mean-field solutions for the complete lattice

In this appendix, we study the solutions for the complete lattice, keeping track of every site instead of lumping them into sublattices. We show that there is a dynamical instability, in which the uniform steady state becomes unstable to perturbations of wavelength 2. The solutions of the complete lattice are the same as the solutions using sublattices, so the antiferromagnetic transition is not an artifact of dividing the lattice into two sublattices.

The approach is to find the uniform steady state and see when it becomes unstable to perturbations. Consider a d -dimensional lattice with N sites in each direction. Let

\vec{n} be a d -dimensional position vector. The system is described by

$$\dot{w}_{\vec{n}} = -2\Omega \operatorname{Im} q_{\vec{n}} - w_{\vec{n}} - 1, \quad (4.35)$$

$$\dot{q}_{\vec{n}} = i \left[\Delta - b \sum_{\langle \vec{m}\vec{n} \rangle} (w_{\vec{m}} + 1) \right] q_{\vec{n}} - \frac{q_{\vec{n}}}{2} + i \frac{\Omega}{2} w_{\vec{n}}, \quad (4.36)$$

where $b = V/2\gamma = c/2d$ is the nearest-neighbor interaction.

The uniform steady state ($w_{\vec{n}} = w$, $q_{\vec{n}} = q$) is given by the fixed points of the system,

$$\dot{w} = -2\Omega \operatorname{Im} q - w - 1, \quad (4.37)$$

$$\dot{q} = i [\Delta - 2db(w + 1)] q - \frac{q}{2} + i \frac{\Omega}{2} w. \quad (4.38)$$

These equations are the same as Eqs. (4.24)–(4.25) but with $c = 2db$. Thus, we can use the results of Section 4.A.2.1. The uniform steady state is given by the real roots of $f(w)$ in Eq. (4.20), and there are one or three solutions. The Jacobian of Eqs. (4.37)–(4.38) determines the stability of a uniform solution to uniform perturbations, i.e., an identical offset to every site.

Now we consider perturbations $\delta w_{\vec{n}}$, $\delta q_{\vec{n}}$ around the uniform steady state:

$$w_{\vec{n}} = w + \delta w_{\vec{n}}, \quad (4.39)$$

$$q_{\vec{n}} = q + \delta q_{\vec{n}}. \quad (4.40)$$

We write them in terms of Fourier components $\delta\tilde{w}_{\vec{k}}, \delta\tilde{q}_{\vec{k}}$:

$$\delta w_{\vec{n}} = \frac{1}{N} \sum_{\vec{k}} e^{i\vec{k}\cdot\vec{n}} \delta\tilde{w}_{\vec{k}}, \quad (4.41)$$

$$\delta q_{\vec{n}} = \frac{1}{N} \sum_{\vec{k}} e^{i\vec{k}\cdot\vec{n}} \delta\tilde{q}_{\vec{k}}, \quad (4.42)$$

$$\vec{k} = (k_1, k_2, \dots, k_d), \quad (4.43)$$

$$k_\ell = \frac{2\pi}{N} j, \quad j = 0, \dots, N-1. \quad (4.44)$$

We write Eqs. (4.35)–(4.36) in terms of $\delta\tilde{w}_{\vec{k}}, \delta\tilde{q}_{\vec{k}}$ and linearize. The Fourier components are uncoupled from each other and each component \vec{k} is described by three differential equations:

$$\delta\dot{\tilde{w}}_{\vec{k}} = i\Omega(\delta\tilde{q}_{\vec{k}} - \delta\tilde{q}_{-\vec{k}}^*) - \delta\tilde{w}_{\vec{k}}, \quad (4.45)$$

$$\delta\dot{\tilde{q}}_{\vec{k}} = -2ibq \left(\sum_{\ell=1}^d \cos k_\ell \right) \delta\tilde{w}_{\vec{k}} + i\frac{\Omega}{2} \delta\tilde{w}_{\vec{k}} + \left\{ i[\Delta - 2db(w+1)] - \frac{1}{2} \right\} \delta\tilde{q}_{\vec{k}}, \quad (4.46)$$

$$\delta\dot{\tilde{q}}_{-\vec{k}}^* = 2ibq^* \left(\sum_{\ell=1}^d \cos k_\ell \right) \delta\tilde{w}_{\vec{k}} - i\frac{\Omega}{2} \delta\tilde{w}_{\vec{k}} + \left\{ -i[\Delta - 2db(w+1)] - \frac{1}{2} \right\} \delta\tilde{q}_{-\vec{k}}^*. \quad (4.47)$$

The characteristic polynomial for component \vec{k} is

$$\begin{aligned} \eta(\lambda) = & \lambda^3 + 2\lambda^2 + \left\{ [\Delta - 2db(w+1)]^2 + \Omega^2 + \frac{5}{4} - 4\Omega b \operatorname{Re} q \sum_{\ell=1}^d \cos k_\ell \right\} \lambda \\ & + [\Delta - 2db(w+1)]^2 + \frac{\Omega^2}{2} + \frac{1}{4} - 4\Omega b \operatorname{Re} q \sum_{\ell=1}^d \cos k_\ell. \end{aligned} \quad (4.48)$$

Note the similarity to Eqs. (4.27) and (4.28). Now we use the Routh-Hurwitz criterion given in Section 4.A.2. For $\eta(\lambda)$, $a_2 > 0$ and $a_2 a_1 - a_0 = a_0 + \Omega^2 + 2$. Thus, the uniform steady state is stable to a perturbation with wave vector \vec{k} if and only if

$$[\Delta - 2db(w + 1)]^2 + \frac{\Omega^2}{2} + \frac{1}{4} - 4\Omega b \operatorname{Re} q \sum_{\ell=1}^d \cos k_\ell > 0. \quad (4.49)$$

Suppose the uniform steady state satisfies $4\Omega b \operatorname{Re} q > 0$. As the parameters change, the first mode to go unstable is the one with all $k_\ell = 0$. This corresponds to uniform perturbations that simply offset the uniform solution. Thus we identify this uniform steady state as the unstable fixed point of Eqs. (4.37)–(4.38). Based on the discussion in Section 4.A.2.1, this uniform solution is actually always unstable when it exists.

Now suppose the uniform steady state satisfies $4\Omega b \operatorname{Re} q < 0$. As the parameters change, the first mode to go unstable is the one with all $k_\ell = \pi$. This corresponds to perturbations of wavelength 2, i.e., antiferromagnetic perturbations. The uniform steady state is unstable to this mode when

$$[\Delta - 2db(w + 1)]^2 + \frac{\Omega^2}{2} + \frac{1}{4} + 4\Omega db \operatorname{Re} q > 0. \quad (4.50)$$

This is the same as Eq. (4.29) with $c = 2db$. Thus, the discussion in Section 4.A.4 applies here: as the parameters change, the uniform solution becomes unstable to the antiferromagnetic solution. One can find the antiferromagnetic solution, but that is equivalent to the nonuniform fixed points of Eqs. (4.12)–(4.15), i.e., the real roots of

$g(w)$ in Eq. (4.21).

Thus, the complete lattice has the same antiferromagnetic transition as the bipartite lattice.

Chapter 5

Collective quantum jumps of Rydberg atoms

In this chapter, we consider the same setup as in Chapter 4: a group of atoms laser-driven to the Rydberg state and spontaneously decaying back to the ground state. But this time, we study the dynamics using the method of quantum trajectories. In particular, we are interested in what happens in the original quantum model when mean-field theory predicts bistability of uniform fixed points. It turns out that the system jumps between the two stable fixed points of mean-field theory. The jumps are inherently collective and in fact exist only for a large number of atoms. We explain how entanglement and quantum measurement enable the jumps, which are otherwise classically forbidden. The results of this chapter were published in Ref. [48].

5.1 Model

The model is the same as in Chapter 4, except that we are now interested in the long-range type of coupling ($V \sim 1/R^3$). This way, we can ignore the nonuniform fixed

points, which would otherwise complicate the dynamics.¹ The long-range type of coupling can be obtained by a Förster resonance or by applying a static electric field. However, to be able to simulate large systems, we approximate the long-range coupling as a constant all-to-all coupling with suitable normalization; this approximation is appropriate for a two- or three-dimensional lattice for the system sizes used here. In Section 5.5, we discuss what happens with a more-realistic type of coupling.

Consider a system of N atoms continuously excited by a laser from the ground state $|g\rangle$ to a Rydberg state $|e\rangle$. The Hamiltonian in Eq. (4.1) is modified to be

$$H = \sum_j \left[-\Delta |e\rangle\langle e|_j + \frac{\Omega}{2} (|e\rangle\langle g|_j + |g\rangle\langle e|_j) \right] + \frac{V}{N-1} \sum_{j<k} |e\rangle\langle e|_j \otimes |e\rangle\langle e|_k, \quad (5.1)$$

where $\Delta = \omega_\ell - \omega_o$ is the detuning between the laser and transition frequencies and Ω is the Rabi frequency, which depends on the laser intensity. As in Chapter 4, each atom is approximated as a two-level system, and we account for spontaneous emission from the Rydberg state using the linewidth γ . Note that each atom emits into different electromagnetic modes due to the large inter-particle distance; this is an important difference with the Dicke model [70].

The environment absorbs all the spontaneously emitted photons, so the atoms are continuously monitored by the environment. We are interested in the temporal properties of the emitted photons. As discussed in Chapter 2, there are two equivalent ways to study such an open quantum system. The first is the master equation, which

¹But it would be interesting to do a similar study of the nonuniform fixed points.

describes how the density matrix of the atoms, ρ , evolves in time:

$$\dot{\rho} = -i[H, \rho] + \gamma \sum_j \left(-\frac{1}{2} \{ |e\rangle\langle e|_j, \rho \} + |g\rangle\langle e|_j \rho |e\rangle\langle g|_j \right).$$

A master equation of this form has a unique steady-state solution [75], ρ_{ss} , which can be found numerically by Runge-Kutta integration. The integration can be vastly sped up by utilizing the fact that the atoms are symmetric under interchange due to all-to-all coupling; the complexity is then $O(N^3)$ instead of $O(4^N)$. Using ρ_{ss} , one can calculate the statistics of the emitted light. In particular, the correlation of photons emitted by two different atoms is [76]

$$g_{ij}^{(2)} = \frac{\langle E_i E_j \rangle}{\langle E_i \rangle \langle E_j \rangle}, \quad (5.2)$$

where $E_i \equiv |e\rangle\langle e|_i$. If $g_{ij}^{(2)} > 1$, the atoms tend to emit in unison (bunching); if $g_{ij}^{(2)} < 1$, they avoid emitting in unison (antibunching).

The second approach is the method of quantum trajectories, which simulates how the wave function evolves in a single experiment [18, 61, 23]. We describe the quantum-trajectory algorithm in the context of the Rydberg model. Given the wave function $|\psi(t)\rangle$, one randomly decides whether an atom emits a photon in the time interval $[t, t + \delta t]$ based on its current Rydberg population. If atom j emits a photon, the wave function is collapsed: $|\psi(t + \delta t)\rangle = |g\rangle\langle e|_j |\psi(t)\rangle$. If no atoms emit a photon, $|\psi(t + \delta t)\rangle = (1 - iH_{\text{eff}}\delta t)|\psi(t)\rangle$, where $H_{\text{eff}} = H - (i\gamma/2) \sum_j |e\rangle\langle e|_j$. After normalizing the wave function, the process is repeated for the next time step. The non-Hermitian

part of H_{eff} is a shortcut to account for the fact that *the non-detection of a photon shifts the atoms toward the ground state*, as discussed in Section 2.1.

These two approaches are related: the master equation describes an ensemble of many individual trajectories [18, 61]. Also, ρ_{ss} can be viewed as the ensemble of wave functions that a single trajectory explores over time. We use both approaches below, although quantum jumps are most clearly seen using quantum trajectories.

5.2 Case of $N = 2$ atoms

We first consider the case of $N = 2$ atoms since it is instructive for larger N . Laser excitation and spontaneous emission distribute population throughout the Hilbert space, $\{|gg\rangle, |ge\rangle, |eg\rangle, |ee\rangle\}$. When $\Delta = 0$, $|ee\rangle$ is uncoupled from the other states due to its energy shift, so there is little population in it (Fig. 5.1(a)); this is the well-known blockade effect [57, 73]. But when $\Delta \approx V/2$, there is a resonant two-photon transition between $|gg\rangle$ and $|ee\rangle$, so $|ee\rangle$ becomes populated (Fig. 5.1(b)). Using the master equation, one can calculate the photon correlation between the two atoms (Fig. 5.2). There is strong antibunching for $\Delta \approx 0$ and strong bunching for $\Delta \approx V/2$, because a joint emission requires population in $|ee\rangle$. In the limit of small Ω , the correlation is

$$g_{12}^{(2)} = \frac{\gamma^2 + 4\Delta^2}{\gamma^2 + (V - 2\Delta)^2} + \frac{4V(V - 4\Delta)\Omega^2}{[\gamma^2 + (V - 2\Delta)^2]^2} + O(\Omega^4/\gamma^4). \quad (5.3)$$

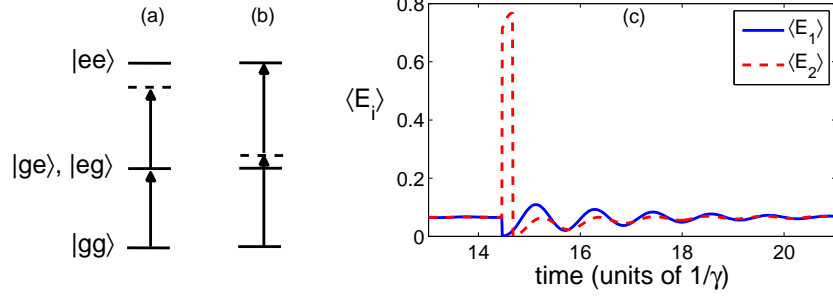


Figure 5.1: Two atoms. (a) When $\Delta = 0$, $|ee\rangle$ is uncoupled from the other states. (b) When $\Delta = V/2$, there is a resonant two-photon transition between $|gg\rangle$ and $|ee\rangle$. (c) Quantum trajectory simulation with $\Omega = 1.5\gamma$, $\Delta = V/2 = 5\gamma$, showing Rydberg population of each atom over time. Atom 1 (solid blue line) emits at $t = 14.4/\gamma$, which causes $\langle E_2 \rangle$ (dashed red line) to suddenly increase. Atom 2 then emits at $t = 14.7/\gamma$. When no photons have been emitted for a while, the wave function approaches a steady state.

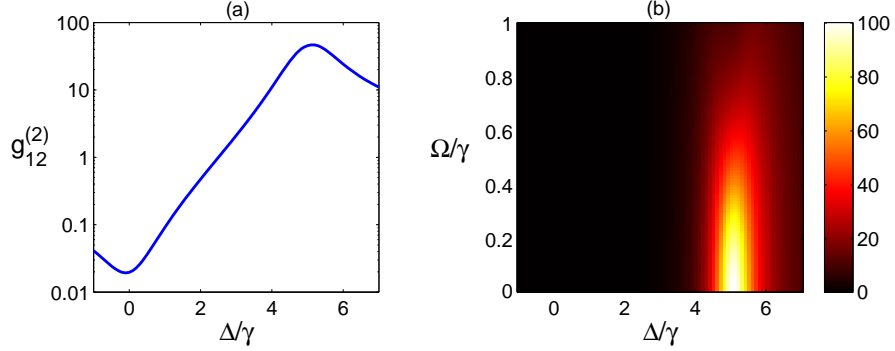


Figure 5.2: Photon correlation for $N = 2$ atoms with $V = 10\gamma$. (a) Correlation vs Δ for $\Omega = 0.5\gamma$. (b) Correlation as a function of Ω and Δ using color scheme on right

Note that the correlation can be made arbitrarily large by setting $\Omega \approx 0$, $\Delta = V/2$, and V large; this may be useful as a heralded single-photon source [25].

Further insight is provided by quantum trajectories. An example trajectory for $\Delta = V/2$ is shown in Fig. 5.1(c). The atoms emit photons at various times. When no photons have been emitted for a while, the wave function approaches an entangled steady state due to the balance of laser excitation and nonunitary decay from the

non-detection of photons:

$$|\psi\rangle_{ss} = c_1|gg\rangle + c_2|ge\rangle + c_3|eg\rangle + c_4|ee\rangle, \quad (5.4)$$

where the coefficients have constant magnitudes and their phases evolve with the same frequency. A similar thing happens with a single atom, as discussed in Section 2.3. Mathematically, the steady-state wave function is the eigenvector of H_{eff} corresponding to the eigenvalue with least negative part. Because of the laser detuning, $|c_1|^2$ is much larger than $|c_2|^2, |c_3|^2, |c_4|^2$, which are comparable to each other. Thus $\langle E_1 \rangle, \langle E_2 \rangle \approx 0$ and the atoms are unlikely to emit. But when atom 1 happens to emit, the wave function becomes

$$|\psi\rangle = \frac{c_3|gg\rangle + c_4|ge\rangle}{|c_3|^2 + |c_4|^2}. \quad (5.5)$$

Now, $\langle E_2 \rangle$ is large and atom 2 is likely to emit, which leads to photon bunching (Fig. 5.1(c)).

5.3 Case of $N = 16$ atoms

Now we consider the case of large N . We first review mean-field theory, which was discussed in Chapter 4, but here we adapt it to use Eq. (5.1). Mean-field theory is a classical approximation to the quantum model: correlations between atoms are ignored, and the density matrix factorizes by atom, $\rho = \bigotimes_{j=1}^N \bar{\rho}$, where $\bar{\rho}$ evolves

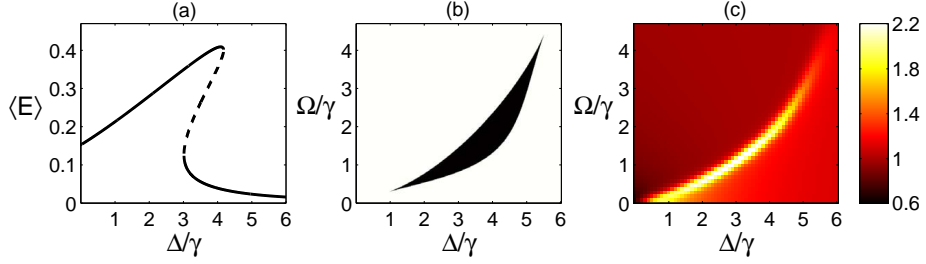


Figure 5.3: (a) Fixed points of mean-field model as function of detuning for $\Omega = 1.5\gamma$ and $V = 10\gamma$. Stable (unstable) fixed points are denoted by solid (dashed) lines. (b) Mean-field bistable region (black) for $V = 10\gamma$. (c) Photon correlation $g_{ij}^{(2)}$ for 16 atoms with same parameters as (b), using color scheme on right

according to

$$\dot{\bar{\rho}}_{ee} = -\Omega \text{Im} \bar{\rho}_{eg} - \gamma \bar{\rho}_{ee}, \quad (5.6)$$

$$\dot{\bar{\rho}}_{eg} = i(\Delta - V\bar{\rho}_{ee})\bar{\rho}_{eg} - \frac{\gamma}{2}\bar{\rho}_{eg} + i\Omega \left(\bar{\rho}_{ee} - \frac{1}{2} \right). \quad (5.7)$$

These are the optical Bloch equations for a two-level atom, except that the effective laser detuning is $\Delta_{\text{eff}} = \Delta - V\bar{\rho}_{ee}$. There are one or two stable fixed points, depending on the parameters (Fig. 5.3(a)). Classically, the system should go to a stable fixed point and stay there, since there are no other attracting solutions.

Now we consider the original quantum model for large N . Figure 5.4(a) shows a quantum trajectory for $N = 16$ and plots the average Rydberg population of all the atoms, $\langle E \rangle$, where $E \equiv \sum_i E_i/N$. $\langle E \rangle$ appears to switch in time between two values. In fact, these two values correspond to the two stable fixed points of mean-field theory for the chosen parameters. Thus, we find that the quantum model jumps between the two stable states of the classical model. When the parameters are such that mean-field theory is monostable, $\langle E \rangle$ remains around one value and there are

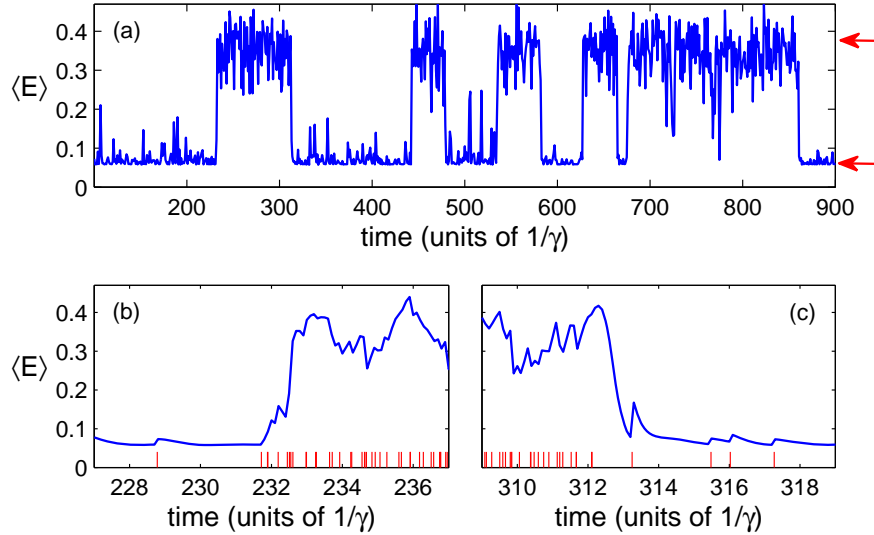


Figure 5.4: Quantum trajectory of 16 atoms showing average Rydberg population over time with $\Omega = 1.5\gamma$, $V = 10\gamma$, $\Delta = 3.4\gamma$. (a) Quantum jumps between two metastable collective states. Red arrows point at the stable fixed points of mean-field theory. (b) and (c) are zoomed-in views, and red lines mark photon emissions. (b) Rapid succession of emissions around $t = 232/\gamma$ causes a jump up. (c) Absence of emissions around $t = 313/\gamma$ causes a jump down.

no jumps. Hence, the photons are bunched when mean-field theory is bistable but are uncorrelated otherwise. This correspondence is evident in Fig. 5.3(b)–(c), with better agreement for larger N .

We call the two states in Fig. 5.4(a) the dark and bright states, since the one with lower $\langle E \rangle$ has a lower emission rate. In the dark state, the wave function approaches a steady state, $|\psi\rangle_{ss}$, in between the sporadic emissions. This is due to the balance of laser excitation and non-unitary decay from the non-detection of photons, similar to the case of two atoms. In the bright state, the large Rydberg population brings the system effectively on resonance ($\Delta_{\text{eff}} \approx 0$). The bright state sustains itself because an atom is quickly reexcited after emitting a photon.

Suppose the system is in the dark state. The steady-state wavefunction $|\psi\rangle_{ss}$ is

an entangled state of all the atoms with most population in $|gg\dots g\rangle$. Although $\langle E \rangle$ is small, when an atom happens to emit a photon, $\langle E \rangle$ increases due to the entangled form of $|\psi\rangle_{ss}$. In fact, if more atoms emit within a short amount of time, $\langle E \rangle$ increases further (Fig. 5.5(a)). When enough atoms have emitted such that $\langle E \rangle$ is high, the system is in the bright state and sustains itself there (Fig. 5.4(b)). If too few atoms emitted, the system quickly returns to $|\psi\rangle_{ss}$.

Then suppose the system is in the bright state. There are two ways to jump to the dark state: most of the atoms emit simultaneously or most of the atoms do not emit for a while (the non-detection of photons projects the atoms toward the ground state). For our parameters, simulations indicate that the latter is usually responsible for the jumps down (Fig. 5.4(c)).

The jumps are inherently collective, since they result from joint emissions or joint non-emissions. As N increases, the dark and bright periods become longer and more distinct (Fig. 5.5(b)–(c)). This can be understood intuitively as follows. Suppose the system is in $|\psi\rangle_{ss}$. As N increases, the increment of $\langle E \rangle$ per emission decreases (Fig. 5.5(a)). Thus, for large N , a rapid succession of many emissions is necessary to jump to the bright state. Although the emission rate in the dark state increases with N , the rate of nonunitary decay in H_{eff} also increases with N . The result is that the probability rate of a jump up decreases. Then suppose the system is in the bright state. As N increases, a jump down requires more atoms to not emit in some time interval, so the probability rate of a jump down decreases.

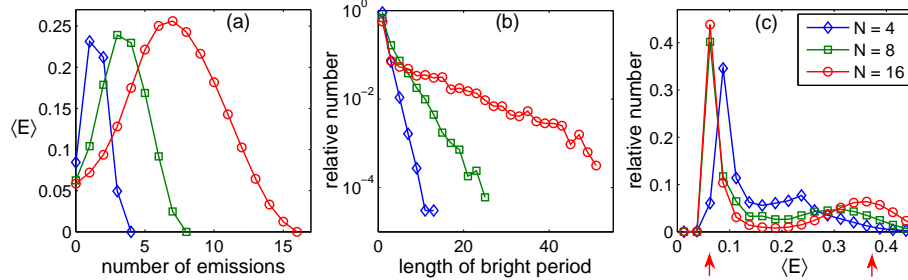


Figure 5.5: Statistics for $\Omega = 1.5\gamma$, $V = 10\gamma$, $\Delta = 3.4\gamma$ comparing $N = 4, 8, 16$. (a) Rydberg population $\langle E \rangle$ after a number of simultaneous emissions from the steady-state wave function $|\psi\rangle_{ss}$. (b) Length distribution of bright periods (in units of $1/\gamma$), using arbitrary threshold of $\langle E \rangle = 0.2$ and sampling rate of 10γ . (c) Distribution of $\langle E \rangle$. Red arrows point at stable fixed points of mean-field theory.

5.4 Experimental considerations

Experimentally, the jumps may be observed in a 2D optical lattice of atoms with a static electric field normal to the plane for long-range Rydberg interaction. For example, two ^{87}Rb atoms in the $|n = 15, q = 14, m = 0\rangle$ Rydberg state have a coupling of about 44 kHz at a distance of $13 \mu\text{m}$ [38], and the linewidth is $\gamma/2\pi \approx 68$ kHz at 0 K [10]. This corresponds to $V \approx 10\gamma$ with $N = 16$ atoms for the all-to-all model in Eq. (5.1), which are the parameters used in our discussion. One could observe the jumps directly by monitoring the fluorescence from the atoms. Alternatively, one could make repeated projective measurements and thereby infer the existence of two metastable states from the distribution of $\langle E \rangle$.

5.5 Conclusion

These collective jumps are reminiscent of a familiar classical effect. It is well known that adding thermal noise to a bistable classical system induces transitions between

the two stable fixed points [24, 1]. In contrast, the jumps here are induced by *quantum* noise due to entanglement and quantum measurement. We note that the jumps may be the many-body version of quantum activation, in which quantum fluctuations drive transitions over a classical barrier [59, 40].

In Eq. (5.1), we assumed an infinite-range coupling for simplicity. One might wonder whether the collective jumps still occur when the coupling is more realistic. A recent work studied the quantum dynamics of the Rydberg model on a one-dimensional chain with nearest-neighbor interactions [5]. They also observed well-defined jumps of the Rydberg population in a chain of $N = 12$ atoms. Thus, for a small system, the existence of jumps does not seem to depend critically on the coupling range. On the other hand, a large system of, say, $N = 1000$ atoms with nearest-neighbor interactions would exhibit more complicated dynamics: the system would probably divide into small domains, and the Rydberg population of a domain would correspond to a mean-field fixed point. The collective jumps would occur on a local scale as domains grow and shrink. The domain-wall dynamics are worth future study.

It would be interesting to see whether similar jumps appear in other settings, such as coupled optical cavities [27, 12, 32, 84] and quantum-reservoir engineering [20, 21, 83, 86]. In particular, since mean-field bistability seems to predict collective jumps in the underlying quantum model, one should look for bistability in the mean-field models of other systems [21, 83, 84]. It is known that a single cavity coupled to an atom is bistable [3]; in fact, jumps between the stable fixed points have been observed recently [41]. It is worth looking at the jump dynamics in an array of cavities.

Chapter 6

Spatiotemporal dynamics of quantum jumps with Rydberg atoms

Chapter 5 showed the Rydberg interaction greatly affects how a group of atoms fluoresce when the atoms are laser-excited from the ground state to a Rydberg state and spontaneously decay back to the ground state. In this chapter, we study what happens when the atoms are laser-excited to a low-lying excited state as well as a Rydberg state. This three-level scheme leads to qualitatively different behavior: the atoms develop strong spatial correlations that change on a long time scale.

Our idea is based on quantum jumps of a three-level atom. As discussed in Section 2.4, an atom driven strongly to a short-lived state and weakly to a metastable state occasionally jumps to and from the metastable state. The jumps are visible in the fluorescence of the strong transition, which exhibits distinct bright and dark periods. Here, we consider a one-dimensional chain of many three-level atoms, and we let the metastable state be a Rydberg state, so that a jump of one atom affects its neighbors' jumps via the Rydberg interaction. This leads to rich spatiotemporal dynamics, which

are observable by imaging the fluorescence of the strong transition. The results of this chapter were published in Ref. [45]

Previous works studied correlated quantum jumps of atoms in the context of the Dicke model [53, 79]. They concluded that cooperative effects are very difficult to see experimentally, because the interatomic distance must be much smaller than a wavelength. In contrast, the strong Rydberg interaction here allows the interatomic distance to be much longer than a wavelength. Thus, the atoms develop strong correlations while being individually resolvable.

6.1 Many-atom model

As discussed in Section 2.4, an atom is assumed to have three states: ground state $|g\rangle$, short-lived excited state $|e\rangle$, and metastable state $|r\rangle$ (Fig. 6.1(a)). In this chapter, we choose the metastable state to be a Rydberg state since Rydberg states have long lifetimes [26]. A laser drives the strong transition $|g\rangle \rightarrow |e\rangle$, while another drives the weak transition $|g\rangle \rightarrow |r\rangle$. Alternatively, one could use a cascade configuration with $|e\rangle \rightarrow |r\rangle$ as the weak transition (see Section 6.4).

We make the following assumptions on the parameters. To avoid power-broadening on the strong transition, we choose to work in the low-intensity limit, $\Omega_e \ll \gamma_e$; this choice is clarified in Section 6.4. As in Section 2.4, for convenience, we set $\Delta_e = 0$, although it may be experimentally useful to set $\Delta_e < 0$ for continuous laser cooling [60]. We also set $\gamma_r = 0$, since the lifetime of the Rydberg state scales as n^3 and hence can be chosen to be arbitrarily long [26]. It is straightforward to extend the analysis

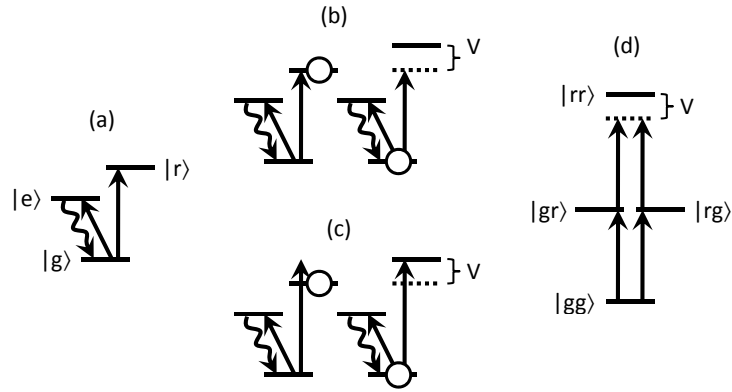


Figure 6.1: (a) An atom has a ground state $|g\rangle$, short-lived excited state $|e\rangle$, and metastable state $|r\rangle$, which is chosen to be a Rydberg state. One observes the spontaneous emission from $|e\rangle$. (b) The $|g\rangle \rightarrow |r\rangle$ transition is originally on resonance ($\Delta_r = 0$), but when one atom is in $|r\rangle$, the other atom is off resonance. (c) The $|g\rangle \rightarrow |r\rangle$ transition is originally off resonance ($\Delta_r = V$), but when one atom is in $|r\rangle$, the other atom is on resonance. (d) When $\Delta_r = 0$, $|rr\rangle$ is weakly coupled to the other states. Note that (b) and (d) are equivalent.

to nonzero Δ_e and γ_r .

We consider a one-dimensional chain of N three-level atoms, which are all uniformly excited on the same two transitions. The interatomic distance is assumed to be large enough so that the fluorescence from each atom is resolvable *in situ* on a camera [7]. The atoms are coupled via the dipole-dipole interaction between their Rydberg states. As discussed in Chapter 3, in the absence of a static electric field, the interaction decreases with the third power of distance for short distances and with the sixth power of distance for long distances. We focus on the latter case, since the example numbers given in Sec. 6.4 are for relatively long distances, although the

former case would also be interesting to study. The Hamiltonian is

$$\begin{aligned}
H = & \sum_i \left[\frac{\Omega_e}{2} (|g\rangle\langle e|_i + |e\rangle\langle g|_i) + \frac{\Omega_r}{2} (|g\rangle\langle r|_i + |r\rangle\langle g|_i) - \Delta_r |r\rangle\langle r|_i \right] \\
& + \sum_{i<j} \frac{V}{|i-j|^6} |r\rangle\langle r|_i \otimes |r\rangle\langle r|_j,
\end{aligned} \tag{6.1}$$

where V is the nearest-neighbor interaction. We have included interactions beyond nearest neighbors in case the long-distance interactions are important; it is known that they affect the many-body ground state of Eq. (6.1) when $\Omega_e = 0$ [77].

To demonstrate the rich spatiotemporal dynamics of the many-body system, Fig. 6.2 shows simulations of a chain of $N = 8$ atoms, generated using the method of quantum trajectories [18, 61]. Each trajectory simulates a single experimental run. The simulations use periodic boundary conditions and include interactions up to the third neighbor. Figure 6.2 plots the time evolution of the Rydberg population of each atom, i.e., the expectation value of $R_i \equiv |r\rangle\langle r|_i$. The atoms undergo quantum jumps, and the Rydberg interaction clearly leads to spatial correlations in the fluorescence.

There are different types of collective dynamics depending on the parameters. In Fig. 6.2(a)–(b), $\Omega_r \ll \Omega_e^2/\gamma_e$, so an atom by itself would exhibit quantum jumps. In Fig. 6.2(a) ($\Delta_r = 0$), a dark period usually does not spread to the neighboring atoms. But once in a while, a dark period does spread to the neighbors, so that there are two or three dark atoms in a row (e.g., *BDDB*). When there are multiple dark atoms in a row, they stay dark for a relatively long time. In Fig. 6.2(b) ($\Delta_r = V$), once a dark spot is created, it spreads quickly to the neighboring atoms. The dark region expands and contracts in size and appears to diffuse along the chain. Interestingly,

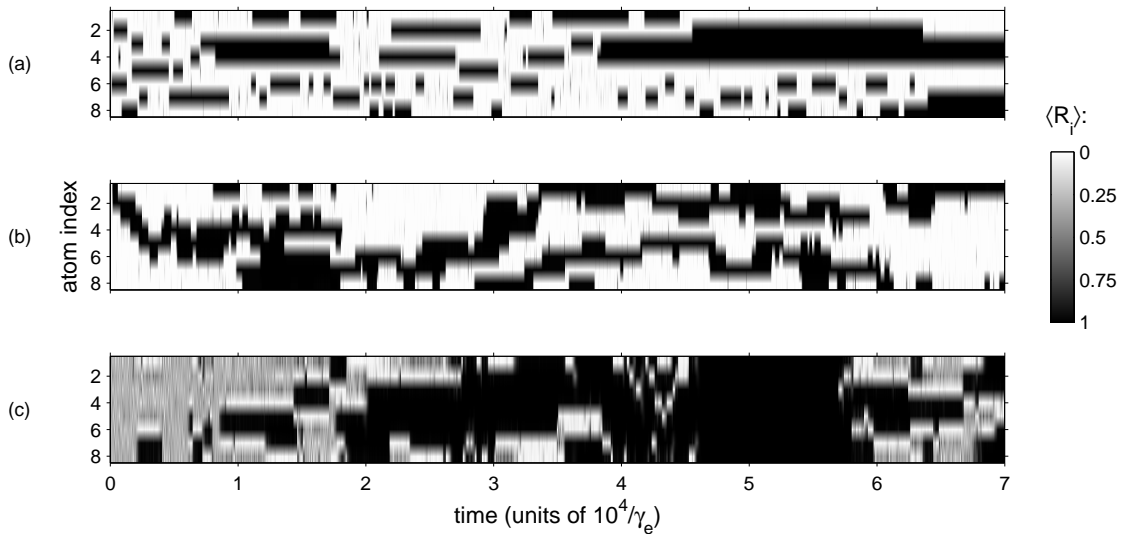


Figure 6.2: Quantum trajectory simulation of a chain of $N = 8$ atoms with periodic boundary conditions. The Rydberg population of each atom is plotted vs. time, using color scheme on the right. White color means that the atom is bright and not in the Rydberg state. Black color means that the atom is dark and in the Rydberg state. (a) $\Omega_e = 0.2\gamma_e$, $\Omega_r = 0.005\gamma_e$, $\Delta_r = 0$, $V = 0.1\gamma_e$. (b) $\Omega_e = 0.2\gamma_e$, $\Omega_r = 0.005\gamma_e$, $\Delta_r = V = 0.1\gamma_e$. (c) $\Omega_e = \Omega_r = 0.1\gamma_e$, $\Delta_r = 0$, $V = 0.4\gamma_e$.

when two dark regions are close to each other, they usually do not merge, but appear to “repel” each other. In Fig. 6.2(c) ($\Omega_r = \Omega_e$, $\Delta_r = 0$), the atoms tend to turn dark or bright in groups of two or three, and sometimes all the atoms are dark. The existence of jumps here is surprising because a single atom would not exhibit jumps for these parameters.

To understand the results for $N = 8$, it is instructive to consider the simpler case of $N = 2$ atoms. Figure 6.3 shows quantum trajectory simulations for $N = 2$; note the similarity with Fig. 6.2. We have analytically solved the $N = 2$ case, and the details are in Appendices 6.A and 6.B. In the next two sections, we summarize the $N = 2$ results and relate them back to the $N = 8$ simulations. There are two general cases: (i) $\Omega_r \ll \Omega_e^2/\gamma_e$ and (ii) $\Omega_r = \Omega_e$, $\Delta_r = 0$, distinguished by whether or not a

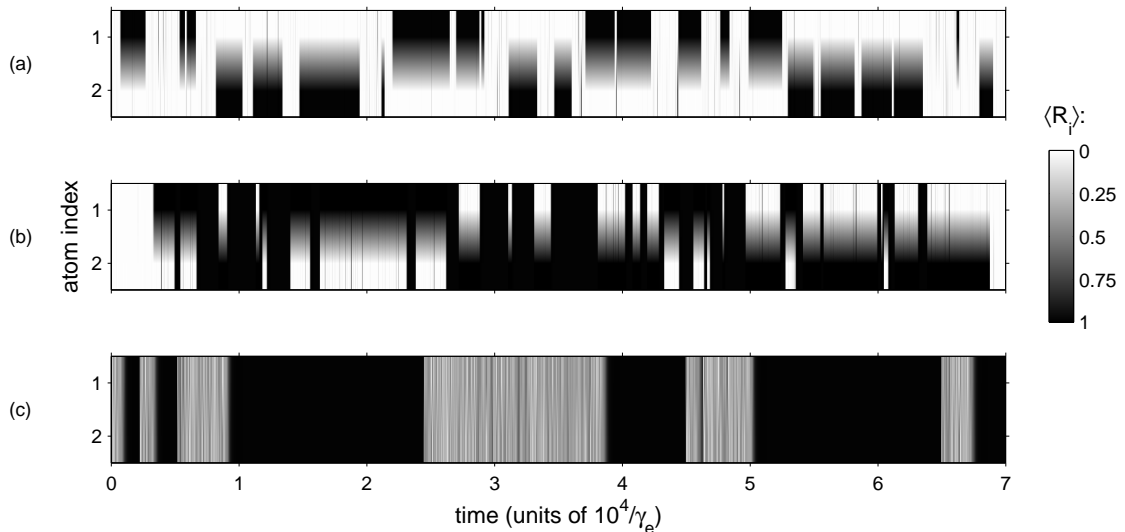


Figure 6.3: Quantum trajectory simulation of $N = 2$ atoms. The Rydberg population of each atom is plotted vs. time, using color scheme on the right. Parameters are the same as in Fig. 6.2: (a) $\Omega_e = 0.2\gamma_e$, $\Omega_r = 0.005\gamma_e$, $\Delta_r = 0$, $V = 0.1\gamma_e$. (b) $\Omega_e = 0.2\gamma_e$, $\Omega_r = 0.005\gamma_e$, $\Delta_r = V = 0.1\gamma_e$. (c) $\Omega_e = \Omega_r = 0.1\gamma_e$, $\Delta_r = 0$, $V = 0.4\gamma_e$.

single atom would exhibit jumps.

6.2 Case of $\Omega_r \ll \Omega_e^2/\gamma_e$

For these parameters, an atom by itself would exhibit jumps. Let the two atoms be labelled 1 and 2. If atom 1 is in $|r\rangle$, then according to Eq. (6.1), atom 2 effectively sees a laser detuning of $\Delta_r - V$. But if atom 1 is not in $|r\rangle$, then atom 2 sees the original detuning Δ_r . Whether atom 1 is in $|r\rangle$ depends on whether it is in a dark period. This suggests that the jump rates for atom 2 are the same as for a single atom (Eqs. (2.11)–(2.12)), except with an effective detuning that depends on whether atom 1 is in a bright or dark period at the moment. In Appendix 6.A, we use a more careful analysis to show that this is indeed correct in the limit of small Ω_r . Thus, the

transition rates for two atoms are

$$\Gamma^{BB \rightarrow BD}(\Delta_r) = \Gamma^{BB \rightarrow DB}(\Delta_r) = \Gamma^{B \rightarrow D}(\Delta_r) \quad (6.2)$$

$$\Gamma^{BD \rightarrow BB}(\Delta_r) = \Gamma^{DB \rightarrow BB}(\Delta_r) = \Gamma^{D \rightarrow B}(\Delta_r) \quad (6.3)$$

$$\Gamma^{BD \rightarrow DD}(\Delta_r) = \Gamma^{DB \rightarrow DD}(\Delta_r) = \Gamma^{B \rightarrow D}(\Delta_r - V) \quad (6.4)$$

$$\Gamma^{DD \rightarrow BD}(\Delta_r) = \Gamma^{DD \rightarrow DB}(\Delta_r) = \Gamma^{D \rightarrow B}(\Delta_r - V). \quad (6.5)$$

An insightful quantity is the ratio $\Gamma^{BD \rightarrow DD} / \Gamma^{BD \rightarrow BB}$, which indicates how often DD periods occur relative to BB periods. As shown in Fig. 6.4, the ratio is minimum at $\Delta_r = 0$ and maximum at $\Delta_r = V$.

The minimum at $\Delta_r = 0$ is due to the blockade effect: although the laser is originally on resonance, when atom 1 is in $|r\rangle$, it shifts the Rydberg level of atom 2 off resonance so that atom 2 is prevented from jumping to $|r\rangle$ (Fig. 6.1(b)). Thus, the atoms switch between BB , BD , and DB ; they are almost never in DD . In other words, there is at most one dark atom at a time (Fig. 6.3(a)).

The maximum at $\Delta_r = V$ is due to the opposite effect: the laser is originally off

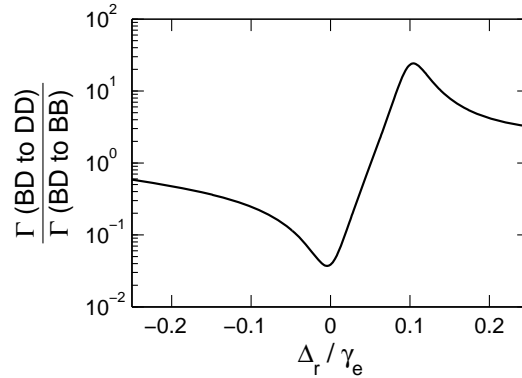


Figure 6.4: Ratio of $\Gamma^{BD \rightarrow DD}$ to $\Gamma^{BD \rightarrow BB}$ for $\Omega_e = 0.2\gamma_e$, $\Omega_r = 0.005\gamma_e$, $V = 0.1\gamma_e$

resonance, but when atom 1 happens to jump to $|r\rangle$, it brings the Rydberg level of atom 2 on resonance, encouraging atom 2 to jump to $|r\rangle$ (Fig. 6.1(c)). Thus, the atoms switch between DD , BD , and DB ; they are almost never in BB , except for the initial transient. Since

$$\frac{\Gamma^{DD \rightarrow BD} + \Gamma^{DD \rightarrow DB}}{\Gamma^{BD \rightarrow BB} + \Gamma^{BD \rightarrow DD}} \approx 2, \quad (6.6)$$

a DD period is shorter than a BD or DB period by about a factor of two. When the atoms are in DD , there is an equal chance to go to BD or DB . Thus, the dark spot appears to do a random walk between the two atoms (Fig. 6.3(b)).

The above considerations can be generalized to larger N . The transition rates for atom i are given by Eqs. (2.11)–(2.12) but with an effective detuning that depends on the number of nearest neighbors that are currently dark: $\Delta_{\text{eff}} = \Delta_r - V \times$ number of dark neighbors. This analytical prediction agrees with quantum trajectory simulations of $N = 8$ atoms: Fig. 6.5 plots the rates of expansion ($\Gamma^{DBB \rightarrow DDB}$), contraction ($\Gamma^{DDB \rightarrow DBB}$), and merging ($\Gamma^{DBD \rightarrow DDD}$) of dark regions. The agreement implies that interactions beyond nearest neighbors in Eq. (6.1) do not play an important role in the dynamics.

When $\Delta_r = 0$, the blockade effect prevents dark periods from spreading (Fig. 6.2(a)). But once in a while, a dark period does spread to a neighbor and there are two dark atoms in a row (BDD); when this happens, the dark atoms are effectively off resonance, so they stay dark for a long time. In other words, dark regions expand and contract on a long time scale. Note that the expansion and contraction rates decrease

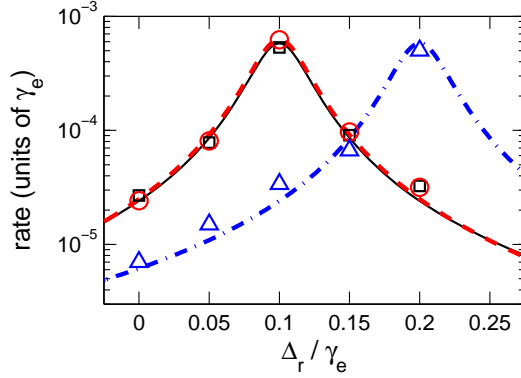


Figure 6.5: Dynamics of dark regions in a chain of $N = 8$ atoms with $\Omega_e = 0.2\gamma_e$, $\Omega_r = 0.005\gamma_e$, $V = 0.1\gamma_e$. The rates of expansion (black squares), contraction (red circles), and merging (blue triangles) were determined from quantum trajectory simulations. The simulation for each value of Δ_r was run for a time of $10^6/\gamma_e$, and the rates were calculated by sampling at a rate of γ_e and defining an atom to be dark if $\langle R_i \rangle > 0.98$. The scatter of data points with low rates is due to statistical uncertainty. Analytical predictions are shown for the rates of expansion (black, solid line), contraction (red, dashed line), and merging (blue, dash-dotted line).

as V increases.

On the other hand, when $\Delta_r = V$, the anti-blockade effect encourages dark periods to spread to the neighbors, causing a dark region to expand (Fig. 6.2(b)). But a dark region usually does not expand enough to encompass the entire chain, because an atom at the edge of a dark region can turn bright, causing the dark region to contract. The expansion and contraction processes have similar rates ($\Gamma^{DBB \rightarrow DDB} \approx \Gamma^{DDB \rightarrow DBB}$). As a result, the dark region appears to diffuse randomly along the chain. Also, two dark regions usually do not merge with each other, i.e., $\Gamma^{DBD \rightarrow DDD}$ is relatively small. This is because a bright atom with two dark neighbors is effectively off resonance and is unlikely to turn dark. Hence, the dark regions appear to repel each other.

6.3 Case of $\Omega_r = \Omega_e$, $\Delta_r = 0$

For these parameters, an atom by itself would not exhibit jumps because of the absence of a weak transition. The existence of jumps for two atoms is solely due to the dipole-dipole interaction, which causes $|gr\rangle \rightarrow |rr\rangle$ and $|rg\rangle \rightarrow |rr\rangle$ to become off-resonant and thus weak transitions (Fig. 6.1(d)). Since $|rr\rangle$ is metastable, the system occasionally jumps to and from $|rr\rangle$. When the system is in $|rr\rangle$, the atoms do not fluoresce. When the system is not in $|rr\rangle$, it turns out that the wavefunction rapidly oscillates among the other eigenstates so that both atoms fluoresce from $|e\rangle$. Thus, the system switches between BB and DD (Fig. 6.3(c)). In Appendix 6.B, we derive the rates,

$$\Gamma^{DD \rightarrow BB} = \frac{\gamma_e \Omega^4}{2V^2(\gamma_e^2 + 4V^2)} \quad (6.7)$$

$$\Gamma^{BB \rightarrow DD} \leq \frac{\Omega^4}{2\gamma_e V^2}, \quad (6.8)$$

where $\Omega \equiv \Omega_r = \Omega_e$. The inequality for $\Gamma^{BB \rightarrow DD}$ is due to incomplete knowledge of the wave function after a photon emission. Equations (6.7)–(6.8) agree well with quantum trajectory simulations (Fig. 6.6). Both rates are inversely related to V , since the weak transitions become weaker as V increases. The condition for well-defined jumps is roughly $\Omega \ll 2V$.

A larger chain has similar behavior (Fig. 6.2(c)). The atoms tend to turn dark or bright simultaneously with their neighbors. However, the dynamics are more complex due to the presence of two neighbors.

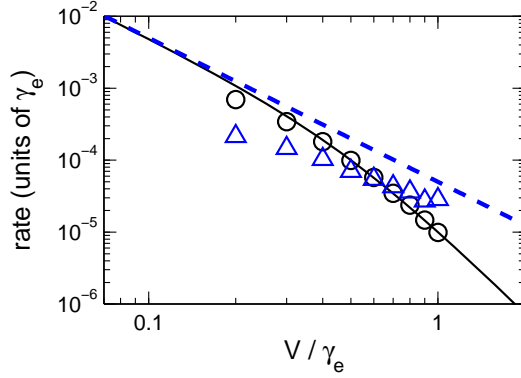


Figure 6.6: Comparison of analytical and numerical values of the jump rates for $\Omega_r = \Omega_e = 0.1\gamma_e$, $\Delta_r = 0$. $\Gamma^{DD \rightarrow BB}$: analytical result (black, solid line) and numerical data (black circles). $\Gamma^{BB \rightarrow DD}$: analytical upper bound (blue, dashed line) and numerical data (blue triangles)

6.4 Experimental considerations

These results can be observed experimentally by using atoms trapped in an optical lattice. For example, one can use ^{87}Rb , which has a strong $5S - 5P$ transition with linewidth $\gamma_e/2\pi = 6$ MHz [60]. Suppose one chooses the $60S$ Rydberg state, which can be reached via a two-photon transition. For a lattice spacing of $7 \mu\text{m}$, the dipole-dipole interaction decreases with the sixth power of distance [73], and the nearest-neighbor interaction is $V = 0.2\gamma_e$ [71]. The lifetime of that Rydberg state is $250 \mu\text{s}$ at 0 K [10]; in other words, $\gamma_r \approx \gamma_e/10^4$. Transitions due to blackbody radiation can be minimized by working at cryogenic temperatures. Also, the nS states have negligible losses from trap-induced photoionization [72, 2]. The trapping of Rydberg atoms in optical lattices was recently demonstrated in Refs. [88, 2].

There is an important constraint on the experimental parameters: the interaction V should be much less than the trap depth, or else the repulsive interaction between two Rydberg atoms will push them out of the lattice. Since a trap depth of 10 MHz

is possible [2], we require $V \ll \gamma_e$. Then to avoid broadening the strong transition [13] and smearing out the effect of V , we choose $\Omega_e \ll \gamma_e$, as stated in Section 6.1.

Instead of using the V configuration in Fig. 6.1(a), one can use a cascade configuration by driving the atom on the $|g\rangle \rightarrow |e\rangle$ and $|e\rangle \rightarrow |r\rangle$ transitions. It is known that quantum jumps occur in this configuration when the upper transition is weak and $|r\rangle$ is metastable [64]. In fact, this is probably the most convenient setup, since experiments often use a two-photon scheme to reach the Rydberg state [92, 35]. To see quantum jumps in a cascade configuration, both transitions should be near resonance instead of far detuned.

6.5 Conclusion

Thus, quantum jumps of Rydberg atoms lead to interesting spatiotemporal dynamics of fluorescence. The next step is to see what happens in larger systems, especially in higher dimensions: what collective behaviors emerge in a large system? It would also be interesting to see what happens when the Rydberg interaction is longer range, i.e., decreasing with the third instead of sixth power of distance; this may lead to significant frustration effects like in equilibrium [77]. Finally, one should study what happens when the atoms are free to move instead of being fixed on a lattice; the combination of electronic and motional degrees of freedom will likely result in rich nonequilibrium behavior.

A potential application of our work is to prepare Rydberg crystals. These are many-body states, in which Rydberg excitations are distributed periodically among

ground-state atoms, e.g., $|grgrgr\rangle$. Rydberg crystals are important for quantum phase transitions, because they are the ground states of the Hamiltonian in Eq. (6.1) with $\Omega_e = 0$ [90, 66, 51, 77]. In addition, they are useful for generating non-classical light [66]. However, they are nontrivial to make, because it is experimentally difficult to address individual atoms to excite them one at a time to the Rydberg state. On the other hand, uniformly exciting all the atoms on the $|g\rangle \rightarrow |r\rangle$ transition leads to complicated collective dynamics [63, 52]. One way to circumvent these difficulties is to uniformly excite all the atoms but adiabatically change the laser detuning to transfer the system to a crystalline state [66]. An alternative approach may be to use quantum jumps by exciting both the $|g\rangle \rightarrow |e\rangle$ and $|g\rangle \rightarrow |r\rangle$ transitions. One would let the atoms jump to and from the Rydberg state while monitoring the fluorescence until the desired crystal is obtained. For example, in Fig. 6.2(a), there is sometimes a $BDBDBD$ pattern. This is in the spirit of recent works that use dissipation to prepare nontrivial quantum states [20]. It is left for future work to study how to optimize the parameters for crystal preparation.

6.A Jump rates for two atoms, $\Omega_r \ll \Omega_e^2/\gamma_e$

In this appendix, we derive the jump rates for $N = 2$ atoms and $\Omega_r \ll \Omega_e^2/\gamma_e$. For these parameters, a single atom would exhibit quantum jumps. In the case of two interacting atoms, each one still undergoes quantum jumps, but the jump rates of each depend on the current state of the other atom. The goal is to calculate, to lowest order in Ω_r , the transition rates among the possible states: BB , BD , DB , and DD .

Suppose for a moment that the interaction strength $V = 0$. Then each atom jumps independently, and the jump rates are the same as the single-atom case (Eqs. (2.11)–(2.12)).

Then let $V \neq 0$. Due to its form, the Rydberg interaction only affects the state $|rr\rangle$. When the atoms are in BB , BD , and DB , there is negligible population in $|rr\rangle$, so the interaction has negligible effect on the transitions among BB , BD , and DB . So to lowest order in Ω_r , those transition rates are the same as when $V = 0$. Thus, we can immediately write down:

$$\Gamma^{BB \rightarrow BD} = \Gamma^{BB \rightarrow DB} = \Gamma^{B \rightarrow D} \quad (6.9)$$

$$\Gamma^{BD \rightarrow BB} = \Gamma^{DB \rightarrow BB} = \Gamma^{D \rightarrow B}. \quad (6.10)$$

The remaining task is to calculate the transition rates that involve DD : $\Gamma^{BD \rightarrow DD}$, $\Gamma^{DB \rightarrow DD}$, $\Gamma^{DD \rightarrow BD}$, and $\Gamma^{DD \rightarrow DB}$.

To calculate these rates, we use an approach similar to Section 2.5. Suppose the atoms are initially in BD , i.e., atom 1 is fluorescing while atom 2 is not. We are interested in the time interval between an emission by atom 1 and a subsequent emission by either atom 1 or 2. Usually the intervals are short since atom 1 is in a bright period. But once in a while, there is a very long interval, which means that atom 1 has become dark and the atoms are in DD . If the long interval ends due to an emission by atom 1, the atoms end up in BD ; if it is due to an emission by atom 2, the atoms end up in DB . We want to calculate $P_0(t)$, which is the probability that neither atom has emitted a photon by time t , given that atom 1 emitted at time 0

and also given that atom 2 started dark. $P_0(t)$ has a long tail corresponding to time spent in DD .

We write $P_0(t) = P_{\text{short}}(t) + P_{\text{long}}(t)$ to separate the short and long time-scale parts. The long tail is given by $P_{\text{long}}(t) = p \exp(-2\Gamma^{DD \rightarrow BD}t)$, where p is the probability that a given interval is long enough to be a DD period. $2\Gamma^{DD \rightarrow BD}$ is the total transition rate out of DD since $\Gamma^{DD \rightarrow BD} = \Gamma^{DD \rightarrow DB}$.

To evolve the wave function in the absence of an emission, we use the non-Hermitian Hamiltonian $H_{\text{eff}} = H - i\frac{\gamma_e}{2}(|e\rangle\langle e|_1 + |e\rangle\langle e|_2)$, where H is the two-atom Hamiltonian. We want to solve the differential equation $i\frac{d}{dt}|\psi(t)\rangle = H_{\text{eff}}|\psi(t)\rangle$ in order to find $P_0(t) = \langle\psi(t)|\psi(t)\rangle$.

The question now is what initial condition to use. Since atom 1 is assumed to emit at time 0, it is in $|g\rangle$. Also, as discussed above, during a BD period, there is very little population in $|rr\rangle$, so the interaction has negligible effect on the dynamics. To first order in Ω_r , atom 2's wave function is the same as that of a single atom in a dark period (Eq. (2.15)). So the initial condition of the two-atom system is:

$$|\psi(0)\rangle = \frac{\Omega_r(-2\Delta_r + i\gamma_e)}{4\Delta_r^2 - \Omega_e^2 - 2i\gamma_e\Delta_r}|gg\rangle + \frac{\Omega_r\Omega_e}{4\Delta_r^2 - \Omega_e^2 - 2i\gamma_e\Delta_r}|ge\rangle + |gr\rangle. \quad (6.11)$$

The general solution to the differential equation is $|\psi(t)\rangle = \sum_n c_n e^{-i\lambda_n t}|u_n\rangle$, where λ_n and $|u_n\rangle$ are the eigenvalues and eigenvectors of H_{eff} , which is a 9×9 matrix. c_n is determined from the initial condition $|\psi(0)\rangle = \sum_n c_n |u_n\rangle$.

We calculate the eigenvalues and eigenvectors perturbatively in Ω_r . All nine eigenvalues have negative imaginary parts, which leads to the nonunitary decay. It turns

out that the imaginary part of one of the eigenvalues, which we call λ_9 , is much less negative than the other eight. This means that the other eight components of $|\psi(t)\rangle$ decay much faster than the $|u_9\rangle$ component. After a long time without a photon emission, $|\psi(t)\rangle$ contains only $|u_9\rangle$. Thus, λ_9 corresponds to the long tail of $P_0(t)$.

To second order in Ω_r ,

$$\lambda_9 = -2\Delta_r + V + \frac{\Omega_r^2(-2\Delta'_r + i\gamma_e)}{4\Delta_r'^2 - \Omega_e^2 - 2i\gamma_e\Delta'_r}, \quad (6.12)$$

where $\Delta'_r = \Delta_r - V$. To first order in Ω_r ,

$$\begin{aligned} |u_9\rangle &= \frac{\Omega_r(-2\Delta'_r + i\gamma_e)}{4\Delta_r'^2 - \Omega_e^2 - 2i\gamma_e\Delta'_r} |gr\rangle + \frac{\Omega_e\Omega_r}{4\Delta_r'^2 - \Omega_e^2 - 2i\gamma_e\Delta'_r} |er\rangle \\ &+ \frac{\Omega_r(-2\Delta'_r + i\gamma_e)}{4\Delta_r'^2 - \Omega_e^2 - 2i\gamma_e\Delta'_r} |rg\rangle + \frac{\Omega_e\Omega_r}{4\Delta_r'^2 - \Omega_e^2 - 2i\gamma_e\Delta'_r} |re\rangle + |rr\rangle \\ c_9 &= \frac{\Omega_r(-2\Delta'_r + i\gamma_e)}{4\Delta_r'^2 - \Omega_e^2 - 2i\gamma_e\Delta'_r}. \end{aligned} \quad (6.13)$$

Note that $|u_9\rangle$ consists mainly of $|rr\rangle$, since it corresponds to a DD period.

We can now construct $P_{\text{long}}(t)$:

$$p = |c_9|^2 \quad (6.14)$$

$$= \frac{\Omega_r^2(\gamma_e^2 + 4\Delta_r'^2)}{16\Delta_r'^4 + 4\Delta_r'^2(\gamma_e^2 - 2\Omega_e^2) + \Omega_e^4} \quad (6.15)$$

$$\Gamma^{DD \rightarrow BD} = \Gamma^{DD \rightarrow DB} = -\text{Im } \lambda_9 \quad (6.16)$$

$$= \frac{\gamma_e\Omega_e^2\Omega_r^2}{16\Delta_r'^4 + 4\Delta_r'^2(\gamma_e^2 - 2\Omega_e^2) + \Omega_e^4}. \quad (6.17)$$

To calculate $\Gamma^{BD \rightarrow DD}$, we use the shortcut from Section 2.5. Since atom 1 is bright,

it has negligible population in $|r\rangle$, so its emission rate Γ_{short} is the same as a two-level atom (Eq. (2.19)). Each emission has probability p of being long enough to be a dark period.

$$\Gamma^{BD \rightarrow DD} = \Gamma^{DB \rightarrow DD} = p \Gamma_{\text{short}} \quad (6.18)$$

$$= \frac{\gamma_e^2 + 4\Delta_r'^2}{\gamma_e^2 + 2\Omega_e^2} \Gamma^{DD \rightarrow BD}. \quad (6.19)$$

Note the similarity between Eqs. (6.17) and (2.11) and between Eqs. (6.19) and (2.12)

6.B Jump rates for two atoms, $\Omega_r = \Omega_e$, $\Delta_r = 0$

In this appendix, we derive the jump rates for $N = 2$ atoms and $\Omega_r = \Omega_e$, $\Delta_r = 0$. For these parameters, a single atom would not exhibit quantum jumps. The existence of jumps for two atoms is solely due to the interaction. To calculate the jump rates, we use an approach similar to Section 2.5 and Appendix 6.A, but there are some important differences.

We are interested in the time intervals between photon emissions of either atom. We want to calculate $P_0(t)$, which is the probability that neither atom has emitted a photon by time t , given that atom 1 emitted at time 0. (Alternatively, one could let atom 2 emit at time 0.) We write $P_0(t) = P_{\text{short}}(t) + P_{\text{long}}(t)$ to separate the short and long time-scale parts. As in Appendix 6.A, we want to solve the differential equation $i \frac{d}{dt} |\psi(t)\rangle = H_{\text{eff}} |\psi(t)\rangle$ in order to find $P_0(t) = \langle \psi(t) | \psi(t) \rangle$.

Before discussing what initial condition to use, we first calculate the eigenvalues

λ_n and eigenvectors $|u_n\rangle$ of H_{eff} . We define $\Omega \equiv \Omega_r = \Omega_e$ and do perturbation theory in Ω , which is assumed to be small. As in Appendix 6.A, all nine eigenvalues have negative imaginary parts, which leads to the nonunitary decay. The imaginary part of one of the eigenvalues, which we call λ_9 , is much less negative than the other eight. This means that the other eight components of $|\psi\rangle$ decay much faster than the $|u_9\rangle$ component. Thus, λ_9 corresponds to the long tail of $P_0(t)$. To fourth order in Ω ,

$$\lambda_9 = V + \frac{\Omega^2}{2V} + \frac{\Omega^4(2V - i\gamma_e)}{4V^2(\gamma_e^2 + 4V^2)}. \quad (6.20)$$

To first order in Ω ,

$$|u_9\rangle = \frac{\Omega}{2V}|gr\rangle + \frac{\Omega}{2V}|rg\rangle + |rr\rangle, \quad (6.21)$$

which consists mainly of $|rr\rangle$, reflecting the fact that if both atoms have not emitted for a while, they are in a DD period.

Now it turns out that the real parts of the other eight eigenvalues have very different values, which causes the wave function to oscillate rapidly among the eight eigenvectors. Thus, after atom 1 emits a photon, the short time scale behavior consists of rapid oscillation among the eight eigenvectors, and each atom's $|e\rangle$ population fluctuates a lot. The time scale of the oscillation is faster than the typical photon emission rate, so both atoms are equally likely to emit next. Thus, the atoms can either be in BB or DD . When in BB , both atoms emit, and the time interval between emissions is relatively short. But once in a while, it takes a very long time for the

next photon to be emitted, which means that the atoms are in DD . Once the long interval ends, the atoms go back to BB .

The rapid oscillation during BB makes it impossible to choose a unique initial condition $|\psi(0)\rangle$, because each time atom 1 emits, atom 2's wave function is different. To account for this ignorance, we let atom 2's wave function be completely arbitrary:

$$|\psi(0)\rangle = a_1|gg\rangle + a_2|ge\rangle + a_3|gr\rangle. \quad (6.22)$$

Normalization requires $|a_1|^2 + |a_2|^2 + |a_3|^2 = 1$, but a_1, a_2, a_3 are otherwise unknown. Despite the incomplete knowledge, we can still obtain a useful bound on $\Gamma^{BB \rightarrow DD}$.

The general solution to the differential equation $i\frac{d}{dt}|\psi(t)\rangle = H_{\text{eff}}|\psi(t)\rangle$ is $|\psi(t)\rangle = \sum_n c_n e^{-i\lambda_n t} |u_n\rangle$, where c_n is determined from the initial condition $|\psi(0)\rangle = \sum_n c_n |u_n\rangle$.

To first order in Ω ,

$$c_9 = a_3 \frac{\Omega}{2V}. \quad (6.23)$$

Given the above results, we can now construct $P_{\text{long}}(t) = p \exp(-\Gamma^{DD \rightarrow BB} t)$, where p is the probability that a given interval is long enough to be a DD period, and $\Gamma^{DD \rightarrow BB}$ is the transition rate from DD to BB :

$$p = |c_9|^2 \leq \frac{\Omega^2}{4V^2} \quad (6.24)$$

$$\Gamma^{DD \rightarrow BB} = -2 \text{Im } \lambda_9 \quad (6.25)$$

$$= \frac{\gamma_e \Omega^4}{2V^2(\gamma_e^2 + 4V^2)}. \quad (6.26)$$

The inequality for p reflects the incomplete knowledge of the initial wave function.

To calculate $\Gamma^{BB \rightarrow DD}$, we have to first calculate Γ_{short} , which is the total emission rate of both atoms during a BB period. We approximate Γ_{short} using the emission rate in the absence of the $|g\rangle \rightarrow |r\rangle$ transition, like in Eq. (2.19):

$$\Gamma_{\text{short}} \approx \frac{2\gamma_e \Omega^2}{\gamma_e^2 + 2\Omega^2}. \quad (6.27)$$

However, since the $|g\rangle \rightarrow |r\rangle$ transition is not weak, the above approximation to Γ_{short} is usually an upper bound. Now we can calculate:

$$\Gamma^{BB \rightarrow DD} = p \Gamma_{\text{short}} \leq \frac{\Omega^4}{2\gamma_e V^2}. \quad (6.28)$$

The jumps are well-defined when a BB period consists of many emissions while a DD period consists of the absence of many emissions: $\Gamma^{BB \rightarrow DD}, \Gamma^{DD \rightarrow BB} \ll \Gamma_{\text{short}}$.

Roughly speaking, this happens when

$$\Omega \ll 2V. \quad (6.29)$$

Chapter 7

Conclusion

We have shown that Rydberg atoms are a promising setting to study quantum nonequilibrium physics. An important avenue for future research is the nonequilibrium critical phenomena of this system. In Chapter 4, we used mean-field theory to identify different phases and the transitions between them. The question now is whether long-range order occurs in finite dimensions. Since it is difficult to simulate large systems, one probably needs to develop new analytical techniques to deal with this problem. In addition, experiments could provide much information.

Throughout the thesis, we assumed that the atoms are fixed on a lattice. It would be interesting to study what happens when the atoms are free to move. Experimentally, this is easier to implement than an optical lattice, and many experiments already produce large clouds of cold atoms. The dipole-dipole interaction would lead to an attractive or repulsive force, and there would also be momentum kicks due to spontaneous emission. Thus, the interaction between two atoms would constantly change as the distance between them changes. It is not obvious what collective behavior would emerge when the atoms are not fixed on a lattice. This is reminiscent of classical reaction-diffusion systems that are often studied in the context of chemical

reactions [16].

While we have focused on Rydberg atoms, one should explore nonequilibrium physics in other cold-atom systems. A promising candidate is trapped ions. One can trap several ions in a radio-frequency trap and manipulate their quantum states with lasers. The ions interact via Coulomb repulsion. There has been much interest in using trapped ions for quantum information processing [30]. On the other hand, they can also be used for nonequilibrium physics, since dissipation can come from spontaneous emission or sideband cooling. The question then is how to arrange driving and dissipation in a way so that something interesting happens.

In any case, the field of quantum nonequilibrium physics promises to be very rich.

Bibliography

- [1] J. S. Aldridge and A. N. Cleland. *Phys. Rev. Lett.*, 94:156403, Apr 2005.
- [2] S. E. Anderson, K. C. Younge, and G. Raithel. *Phys. Rev. Lett.*, 107:263001, Dec 2011.
- [3] M. A. Armen and H. Mabuchi. *Phys. Rev. A*, 73:063801, Jun 2006.
- [4] N. W. Ashcroft and N. D. Mermin. *Solid State Physics*. Brooks/Cole, 1976.
- [5] C. Ates, B. Olmos, J. P. Garrahan, and I. Lesanovsky. *Phys. Rev. A*, 85:043620, Apr 2012.
- [6] J. J. B. Anderson and M. Sitharam. *Amer. Math. Monthly*, 105:447, 1998.
- [7] W. S. Bakr, J. I. Gillen, A. Peng, S. Foelling, and M. Greiner. *Nature*, 462:74, 2009.
- [8] J. C. Bergquist, R. G. Hulet, W. M. Itano, and D. J. Wineland. *Phys. Rev. Lett.*, 57:1699–1702, Oct 1986.
- [9] L. Berthier and G. Biroli. *Rev. Mod. Phys.*, 83:587–645, Jun 2011.
- [10] I. I. Beterov, I. I. Ryabtsev, D. B. Tretyakov, and V. M. Entin. *Phys. Rev. A*, 79:052504, May 2009.

- [11] I. Bloch, J. Dalibard, and W. Zwerger. *Rev. Mod. Phys.*, 80:885–964, Jul 2008.
- [12] I. Carusotto, D. Gerace, H. E. Tureci, S. De Liberato, C. Ciuti, and A. Imamoglu. *Phys. Rev. Lett.*, 103:033601, Jul 2009.
- [13] C. Cohen-Tannoudji and J. Dalibard. *Europhys. Lett.*, 1:441, 1986.
- [14] C. Cohen-Tannoudji, J. Dupont-Roc, and G. Grynberg. *Atom-Photon Interactions*. Wiley, New York, 1992.
- [15] R. J. Cook and H. J. Kimble. *Phys. Rev. Lett.*, 54:1023–1026, Mar 1985.
- [16] M. C. Cross and H. Greenside. *Pattern Formation and Dynamics in Nonequilibrium Systems*. Cambridge University Press, Cambridge, 2009.
- [17] M. C. Cross and P. C. Hohenberg. *Rev. Mod. Phys.*, 65:851–1112, Jul 1993.
- [18] J. Dalibard, Y. Castin, and K. Mølmer. *Phys. Rev. Lett.*, 68:580–583, Feb 1992.
- [19] J. O. Day, E. Brekke, and T. G. Walker. *Phys. Rev. A*, 77:052712, May 2008.
- [20] S. Diehl, A. Micheli, A. Kantian, B. Kraus, H. P. Büchler, and P. Zoller. *Nature Phys.*, 4:878, 2008.
- [21] S. Diehl, A. Tomadin, A. Micheli, R. Fazio, and P. Zoller. *Phys. Rev. Lett.*, 105:015702, Jul 2010.
- [22] P. D. Drummond, K. J. McNeil, and D. F. Walls. *Opt. Acta*, 28:211, 1981.
- [23] R. Dum, P. Zoller, and H. Ritsch. *Phys. Rev. A*, 45:4879–4887, Apr 1992.

- [24] M. I. Dykman and M. A. Krivoglaz. *Sov. Phys. JETP*, 50:30, 1979.
- [25] M. D. Eisaman, J. Fan, A. Migdall, and S. V. Polyakov. *Rev. Sci. Instrum.*, 82:071101, 2011.
- [26] T. Gallagher. *Rydberg Atoms*. Cambridge University Press, Cambridge, 1994.
- [27] D. Gerace, H. E. Türeci, A. Imamoglu, V. Giovannetti, and R. Fazio. *Nature Phys.*, 5:281, 2009.
- [28] S. Gleyzes, S. Kuhr, C. Guerlin, J. Bernu, S. Deléglise, U. B. Hoff, M. Brune, J.-M. Raimond, and S. Haroche. *Nature*, 446:297, 2007.
- [29] M. Gross and S. Haroche. *Phys. Rep.*, 93:301–396, 1982.
- [30] H. Häffner, C. Roos, and R. Blatt. *Phys. Rep.*, 469:155–203, 2008.
- [31] J. Han, Y. Jamil, D. V. L. Norum, P. J. Tanner, and T. F. Gallagher. *Phys. Rev. A*, 74:054502, Nov 2006.
- [32] M. J. Hartmann. *Phys. Rev. Lett.*, 104:113601, Mar 2010.
- [33] J. Honer, H. Weimer, T. Pfau, and H. P. Büchler. *Phys. Rev. Lett.*, 105:160404, Oct 2010.
- [34] F. A. Hopf, C. M. Bowden, and W. H. Louisell. *Phys. Rev. A*, 29:2591–2596, May 1984.
- [35] L. Isenhower, E. Urban, X. L. Zhang, A. T. Gill, T. Henage, T. A. Johnson, T. G. Walker, and M. Saffman. *Phys. Rev. Lett.*, 104:010503, Jan 2010.

- [36] W. M. Itano, D. J. Heinzen, J. J. Bollinger, and D. J. Wineland. *Phys. Rev. A*, 41:2295–2300, Mar 1990.
- [37] J. D. Jackson. *Classical Electrodynamics*. Wiley, 1999.
- [38] D. Jaksch, J. I. Cirac, P. Zoller, S. L. Rolston, R. Côté, and M. D. Lukin. *Phys. Rev. Lett.*, 85:2208–2211, Sep 2000.
- [39] J. Jeener. *Phys. Rev. Lett.*, 82:1772–1775, Feb 1999.
- [40] I. Katz, A. Retzker, R. Straub, and R. Lifshitz. *Phys. Rev. Lett.*, 99:040404, Jul 2007.
- [41] J. Kerckhoff, M. A. Armen, and H. Mabuchi. *Opt. Express*, 19:24468, 2011.
- [42] H. J. Kimble, R. J. Cook, and A. L. Wells. *Phys. Rev. A*, 34:3190–3195, Oct 1986.
- [43] C. Kittel and H. Kroemer. *Thermal Physics*. Freeman, New York, 1980.
- [44] T. Lahaye, C. Menotti, L. Santos, M. Lewenstein, and T. Pfau. *Rep. Prog. Phys.*, 72:126401, 2009.
- [45] T. E. Lee and M. C. Cross. arXiv:1202.1508.
- [46] T. E. Lee and M. C. Cross. *Phys. Rev. Lett.*, 106:143001, Apr 2011.
- [47] T. E. Lee, H. Häffner, and M. C. Cross. *Phys. Rev. A*, 84:031402(R), Sep 2011.
- [48] T. E. Lee, H. Häffner, and M. C. Cross. *Phys. Rev. Lett.*, 108:023602, Jan 2012.

- [49] T. E. Lee, G. Refael, M. C. Cross, O. Kogan, and J. L. Rogers. *Phys. Rev. E*, 80:046210, Oct 2009.
- [50] T. E. Lee, H. Tam, G. Refael, J. L. Rogers, and M. C. Cross. *Phys. Rev. E*, 82:036202, Sep 2010.
- [51] I. Lesanovsky. *Phys. Rev. Lett.*, 106:025301, Jan 2011.
- [52] I. Lesanovsky, B. Olmos, and J. P. Garrahan. *Phys. Rev. Lett.*, 105:100603, Sep 2010.
- [53] M. Lewenstein and J. Javanainen. *Phys. Rev. Lett.*, 59:1289–1292, Sep 1987.
- [54] W. Li, I. Mourachko, M. W. Noel, and T. F. Gallagher. *Phys. Rev. A*, 67:052502, May 2003.
- [55] Y.-Y. Lin, N. Lisitza, S. Ahn, and W. S. Warren. *Science*, 290:118, 2000.
- [56] W.-M. Liu. *J. Math. Anal. Appl.*, 182:250, 1994.
- [57] M. D. Lukin, M. Fleischhauer, R. Cote, L. M. Duan, D. Jaksch, J. I. Cirac, and P. Zoller. *Phys. Rev. Lett.*, 87:037901, Jun 2001.
- [58] F. Marquardt, J. G. E. Harris, and S. M. Girvin. *Phys. Rev. Lett.*, 96:103901, Mar 2006.
- [59] M. Marthaler and M. I. Dykman. *Phys. Rev. A*, 73:042108, Apr 2006.
- [60] H. J. Metcalf and P. van der Straten. *Laser Cooling and Trapping*. Springer, New York, 1999.

- [61] K. Mølmer, Y. Castin, and J. Dalibard. *J. Opt. Soc. Am. B*, 10:524–538, Mar 1993.
- [62] W. Nagourney, J. Sandberg, and H. Dehmelt. *Phys. Rev. Lett.*, 56:2797–2799, Jun 1986.
- [63] B. Olmos, R. González-Férez, and I. Lesanovsky. *Phys. Rev. A*, 79:043419, Apr 2009.
- [64] D. T. Pegg, R. Loudon, and P. L. Knight. *Phys. Rev. A*, 33:4085–4091, Jun 1986.
- [65] M. B. Plenio and P. L. Knight. *Rev. Mod. Phys.*, 70:101–144, Jan 1998.
- [66] T. Pohl, E. Demler, and M. D. Lukin. *Phys. Rev. Lett.*, 104:043002, Jan 2010.
- [67] A. Polkovnikov, K. Sengupta, A. Silva, and M. Vengalattore. *Rev. Mod. Phys.*, 83:863–883, Aug 2011.
- [68] M. Porrati and S. Putterman. *Phys. Rev. A*, 39:3010–3030, Mar 1989.
- [69] J. M. Raimond, M. Brune, and S. Haroche. *Rev. Mod. Phys.*, 73:565–582, Aug 2001.
- [70] J. M. Raimond, P. Goy, M. Gross, C. Fabre, and S. Haroche. *Phys. Rev. Lett.*, 49:1924–1927, Dec 1982.
- [71] A. Reinhard, T. C. Liebisch, B. Knuffman, and G. Raithel. *Phys. Rev. A*, 75:032712, Mar 2007.
- [72] M. Saffman and T. G. Walker. *Phys. Rev. A*, 72:022347, Aug 2005.

- [73] M. Saffman, T. G. Walker, and K. Mølmer. *Rev. Mod. Phys.*, 82:2313–2363, Aug 2010.
- [74] T. Sauter, W. Neuhauser, R. Blatt, and P. E. Toschek. *Phys. Rev. Lett.*, 57:1696–1698, Oct 1986.
- [75] S. G. Schirmer and X. Wang. *Phys. Rev. A*, 81:062306, Jun 2010.
- [76] M. O. Scully and M. S. Zubairy. *Quantum Optics*. Cambridge University Press, Cambridge, 1997.
- [77] E. Sela, M. Punk, and M. Garst. *Phys. Rev. B*, 84:085434, Aug 2011.
- [78] R. Shankar. *Principles of Quantum Mechanics*. Springer, New York, 1994.
- [79] C. Skornia, J. von Zanthier, G. S. Agarwal, E. Werner, and H. Walther. *Europhys. Lett.*, 56:665, 2001.
- [80] I. B. Sperstad, E. B. Stiansen, and A. Sudbø. *Phys. Rev. B*, 81:104302, Mar 2010.
- [81] M. M. Sternheim and J. F. Walker. *Phys. Rev. C*, 6:114–121, Jul 1972.
- [82] S. H. Strogatz. *Nonlinear Dynamics and Chaos*. Perseus Books, Cambridge, 1994.
- [83] A. Tomadin, S. Diehl, and P. Zoller. *Phys. Rev. A*, 83:013611, Jan 2011.
- [84] A. Tomadin, V. Giovannetti, R. Fazio, D. Gerace, I. Carusotto, H. E. Türeci, and A. Imamoglu. *Phys. Rev. A*, 81:061801, Jun 2010.

- [85] A. N. Vamivakas, C.-Y. Lu, C. Matthiesen, Y. Zhao, S. Fält, A. Badolato, and M. Atatre. *Nature*, 467:297, 2010.
- [86] F. Verstraete, M. M. Wolf, and J. I. Cirac. *Nature Phys.*, 5:633, 2009.
- [87] R. Vijay, D. H. Slichter, and I. Siddiqi. *Phys. Rev. Lett.*, 106:110502, Mar 2011.
- [88] M. Viteau, M. G. Bason, J. Radogostowicz, N. Malossi, D. Ciampini, O. Morsch, and E. Arimondo. *Phys. Rev. Lett.*, 107:060402, Aug 2011.
- [89] T. Wang, S. F. Yelin, R. Côté, E. E. Eyler, S. M. Farooqi, P. L. Gould, M. Koštrun, D. Tong, and D. Vrinceanu. *Phys. Rev. A*, 75:033802, Mar 2007.
- [90] H. Weimer and H. P. Büchler. *Phys. Rev. Lett.*, 105:230403, Nov 2010.
- [91] P. Werner, K. Völker, M. Troyer, and S. Chakravarty. *Phys. Rev. Lett.*, 94:047201, Jan 2005.
- [92] T. Wilk, A. Gaëtan, C. Evellin, J. Wolters, Y. Miroshnychenko, P. Grangier, and A. Browaeys. *Phys. Rev. Lett.*, 104:010502, Jan 2010.